Study on using CCTV cameras for estimating Total Suspended Sediment in the Khlong Suan Mak River

CEGM3000 - Multidisciplinary Project - 373

Study on using CCTV cameras for estimating Total Suspended Sediment in the Khlong Suan Mak River

by

Floor Machielse (5064872),
Lois Duijkeren (4686047),
Floortje van Ruth (5034965),

Instructor:	Dr. T.A. (Thom) Bogaard
	Assoc. Prof. Dr. Punpim Puttaraksa Mapiam
Project duration:	September, 2024 - November, 2024
Faculty:	Faculty of Civil Engineering and Geosciences, Delft

TU Delft

KU
KASETSART UNIVERSITY

Acknowledgment

We gratefully acknowledge the Capacity Building of KU Students on Internationalization Program (KUCSI) from The International Affairs Division, KU, and the Agricultural Research Development Agency (public organization), Thailand, for their financial support of this project.

We would like to express our deepest gratitude to our professors, Dr. T.A. (Thom) Bogaard and Assoc. Prof. Dr. Punpim Puttaraksa Mapiam, for providing us with the opportunity to undertake this project and for guiding us throughout its execution. Their invaluable feedback, continuous support, and expert insights were essential to the successful completion of this research.

We are also sincerely thankful to the Department of Environmental Engineering for granting us access to the water laboratory, enabling us to conduct our experiments in a well-equipped and supportive environment.

Lastly, we extend our heartfelt appreciation to the Water Resources team under the supervision of Assoc. Prof. Dr. Punpim Puttaraksa Mapiam for their assistance throughout the project. Their support not only contributed significantly to our research but also enriched our personal development. Through their guidance, we experienced Thailand in a meaningful and transformative way, gaining both academic and cultural insights that will stay with us forever.

Contents

1

Abstract

This study explores the feasibility of using CCTV cameras to estimate Total Suspended Sediment (TSS) concentrations in the Khlong Suan Mak River, located in Kamphaeng Phet Province, Thailand. Climate change has led to prolonged dry spells and intense precipitation in Thailand, causing significant sediment transport and deposition issues in river systems and water infrastructure. Traditional methods for monitoring TSS have inherent limitations, prompting the investigation of RGB image processing as a cost-effective alternative.

Time-series RGB images were captured at multiple weir locations along the river, and pixel intensities were analyzed to estimate sediment concentrations. Synoptic and spatial sediment sampling established baseline TSS values and sediment grain size distributions. Additionally, bathymetric profiles of three major reservoirs were developed to assess sediment accumulation patterns.

Preliminary results demonstrated correlations between RGB intensity values, particularly in the green channel, and TSS under controlled conditions. However, field applications faced challenges due to fluctuating light intensities and minimal variability in TSS concentrations. These findings suggest that while RGB imaging shows promise for sediment monitoring, improvements in camera positioning and lighting control are essential. Future research could enhance accuracy by integrating advanced imaging technologies with this approach.

2 Introduction

Due to climate change, Thailand is increasingly experiencing longer, drier periods and more extreme rainfall events with higher precipitation levels. These conditions significantly impact agriculture, industry, and flood management efforts.
To regulate water flow, reservoirs and weirs have been constructed in regions with intensive agriculture or areas vulnerable to flooding. These structures are essential for controlling water supply during extreme weather events and ensuring adequate water availability during periods of high demand.

In the Kamphaeng Phet region of Thailand, several hydraulic structures have been built to address these challenges. The primary source of water in this area is rainfall, with the main streams receiving runoff primarily from the national park. Reservoirs located at the border of the national park temporarily store this water. From these reservoirs, water is distributed through canals to agricultural areas. After irrigation, the water flows into the Khlong Suan Mak River, eventually draining into the Ping River.

During extreme weather events, rainfall can erode stream banks, carrying soil and other materials into the river. The increased water velocity provides sufficient energy to transport sediment downstream. This sediment becomes part of what is known as Total Suspended Solids (TSS): particles suspended in the water. TSS consists of a mixture of soil, organic matter and fine particles that remain in suspension until settling occurs.
Total Suspended Solids (TSS) accumulation is a big bottleneck in water infrastructure that negatively affects the functionality of hydraulic constructions. When rivers with a high TSS value reduces its velocity, TSS has the time to settle. This often happens when a river encounters a construction, like a weir or dam. When the sediment settles it can build op and causes complications. For example, it reduces water conveyance and can cause structural failures. Irrigation canals are particularly prone to blockages from TSS, which not only restrict water flow but also hinder agricultural productivity [5]. Waters that have a high level of TSS can shorten a hydraulic pump's lifespan by corroding its components, raising the possibility of pump failures [8]. Additionally, sediment buildup can result in significant storage loss within reservoirs. What can lead to an increase of water level upstream and enlarge the risk of flooding.[16]. whereas this is the mean concern in our region.

TSS can enter the river along its entire length, but the two sources likely to have the most impact are the Khlong Lan National Park area and the agricultural land, both contributing through soil erosion. The national park is classified as having a moderate landslide risk due to the combination of frequent heavy rainfall and dense vegetation [9]. While landslides are not common, these conditions increase the chance of localized events during intense weather. In addition, a big part of the land in the Kamphaeng Phet Province is used for agriculture, where cassava and rice are the primary crops. Cassava is an environmental steady crops which is favorable in tropical regions. However, cassava is often cultivated through mono-culture, where large gaps between individual plants leave the soil exposed. This increases the risks of soil degradation [6]. This has negative effects on the soil. Some reports have showed that the loss of farmland soil is significant especially when cassava roots are harvested.[17]

Although TSS may originate from both national park and agricultural sources, it is difficult to determine how much influence each source has on the TSS levels in the Suan Mak River. It is also important to be able to document the amount of TSS build up in the reservoirs or in front of the hydraulic constructions. These interests inspire researchers to find new advanced monitoring technologies capable of measuring and tracking TSS levels over time. While remote sensing is already used for water quality tracing, This technology is partly not fully cable in tracing TSS [18], this is due the fact that data collection is limited because of the limitation of the satellite orbit speeds. What results in gaps in available data, especially during cloudy weather or high turbidity events that occur over short timescales.[10]. Due to these deficiencies there is a need to look into different fields of technology to obtain these kind of data. Where there is a growing interests in a low cost and easy to apply in the field.

Previous studies have viewed the possibility of using image processing techniques for river monitoring. This includes the traditional image processing methods from computer vision, but also new techniques with AI [13]. Modern hydrological stations are increasingly being equipped with optical cameras, like Closed-Circuit Television (CCTV) cameras for surveillance. The imagery collected from these systems can be used more broadly than only surveillance. Researchers are currently developing a system where the RGB value of these images can be analysed in order to identify correlations with sediment concentrations in water. This approach aims to estimate sediment levels and monitor suspended sediments within river systems more effectively. This method allows for continuous data collection, when implemented correctly it can offer a broader and maybe more reliable alternative than other techniques. [13].

Given the presumed sediment buildup at various locations within the study area and the potential of this new sediment-tracing approach, this research assignment was developed.

The research aims to determine whether it is feasible to trace and detect varying concentrations of TSS in the Suan Mak River near designated hydraulic structures. The study also seeks to identify the TSS source within the water system and assess accumulated reservoir sediment, allowing for the selection of a location within the study area where further research on elevated turbidity and TSS concentration can be developed.

Research Objectives

Is TSS traceable? Capture a series of RGB images over time at four designated locations to monitor and analyze sediment transport in a natural setting, aiding in understanding sediment dynamics over time.
What is the source of TSS? Identify the origins of sediment causing reservoir siltation in front of hydraulic structures using spatial sediment sampling and synoptic TSS sampling.
How much are the constructions already influenced by TSS accumulation? Create a bathymetric map of the reservoir to establish a baseline for studying sediment deposition.

3 Area description

Before the explanation, the setup of the research, and what experiments are executed where and why, it is important to first visualize the flow and behavior of the relevant water bodies. Understanding the water flow will provide insight into the transport of TSS, sedimentation patterns, and potential sources, and give a better understanding of why hydraulic construction locations are chosen. Throughout this chapter, locations in the research area are described. To assist the reader in visualizing the locations, an overview of the area has been made and is visible in Figure. 3.1.

3.1 Geographical classification

The Khlong Suan Mak River Basin is located in the Kamphaeng Phet Province, Thailand, and plays a vital role in both agricultural and ecological systems. It is situated near important natural areas such as the Klong Wang Chao National Park and Khlong Lan National Park.

3.2 River basin

The Khlong Suan Mak Basin, a sub-basin of the lower Ping River, is located on the right bank of the Ping River in western Kamphaeng Phet Province and spans over an area of around 1200 km^2. The main river in this Basin is called the Suan mak. The basin is divided into three segments based on river slope. The upstream first part of the river extends over a distance of 20 kilometers and flows through the national parks Khlong Lan and Khlong Wang Chao. Here the river has steep slopes of approximately 1:25 due to the mountainous terrain. The midstream has a flatter slope of 1:150 and a length of around 20-70 kilometers. The final segment has a flat almost zero slope running from 70 km to the river's confluence with the Ping River at 110 km.
The basin covers a diverse landscape, with upland forest areas making up about 40% of the basin, while the midstream and downstream sections transition into agricultural plains. These lower regions are prone to flooding and drought.

3.3 Reservoirs

In the research area, seven large reservoirs have been constructed. The locations of the reservoirs are assigned with the letters A to F in the graph 3. The reservoirs are all located on the border of the national park and at the start of the cropland. Two reservoirs, B and C, differ from the others as they are located farther from the national park area and closer to agricultural land. The majority of the water collected by the reservoirs, therefore, originates from the national park. The reservoirs that have been analyzed for this research are reservoirs A, B, and C. Reservoir A is the largest, with a maximum length and width of approximately 1700 meters and 912 meters, respectively. Reservoir B has a length of 1200 meters and a width of 290 meters. Reservoir C measures 715 meters in length and 604 meters in width.

3.4 Hydraulic constructions

The hydraulic structures are situated along the Suan Mak River, the primary focus of this study. These structures are placed here by the irrigation department for flood prevention and research purposes. These locations are of interest for our research because they are already equipped with CCTV cameras for surveillance, which can be used by us as time series data for sediment flow. Below are the names of the locations, listed in order from 1 to 4. Location 1 is situated downstream, and location 4 is the most upstream of the river.

- Location 1: Tha Kra Dan Weir
- Location 2: Tha Kra Nae Weir
- Location 3: Nong Ping Kai Weir
- Location 4: Khlong Suan Mak Weir

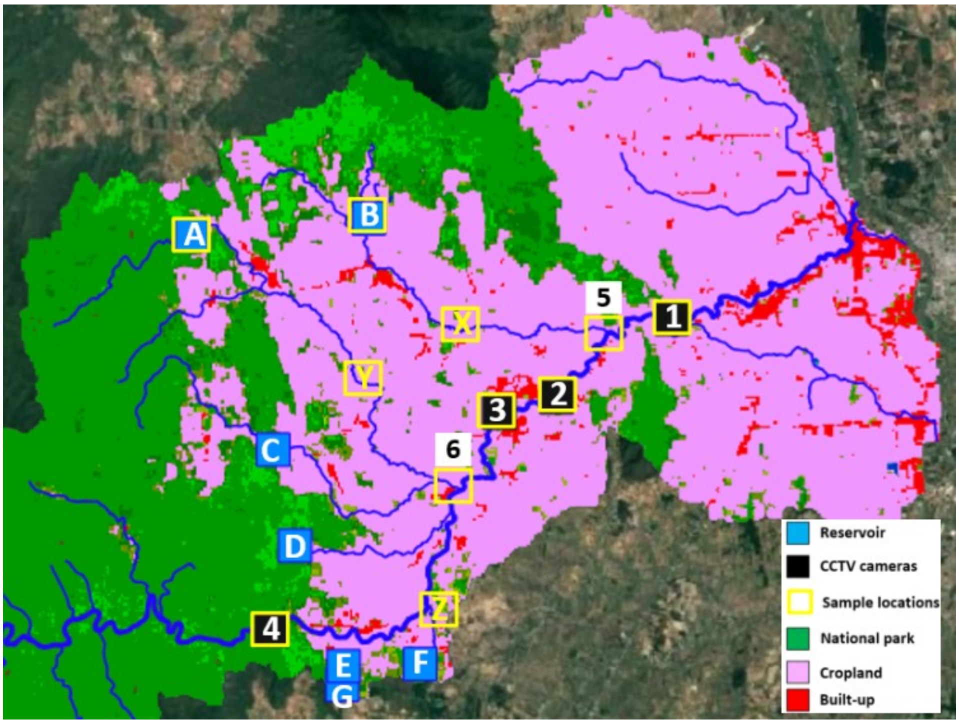

Figure 3.1: Overview of the research area.

4 Methodology

4.1 Sediment experiment procedure

An amount of Suspended Sediment (SS) was collected from the study area. Known quantities of this suspended sediment were dissolved in a white bucket. The concentrations were increased from 0 to 0.7 g/L in steps of 0.1, and then further increased to 1.0, 1.25, and 1.5 g/L. A camera was positioned at a 0-degree angle (vertical) at various distances to observe the effect of increasing distance on suspended sediment detectability.
For each photo image, the water surface was cropped which excluded disturbances as light reflectance or turbulence. The average Red, Green, Blue (RGB) pixel intensities (Pixel Intensity (PI)) were determined according to Equation 4.1.

$$PI_{\text{average},i} = \frac{\sum(i\text{Pixel Intensity})}{\sum(\text{pixels})} \quad \text{with } i = \text{Red, Green, Blue} \tag{4.1}$$

4.2 RGB images constructions processing procedure

In Figure 4.1, the schematization of RGB image processing is presented. Initially, data collection was conducted in the field, followed by two simultaneous steps: laboratory tests of water samples and RGB image processing. The output data from both steps are then combined and visualized in 5.2.

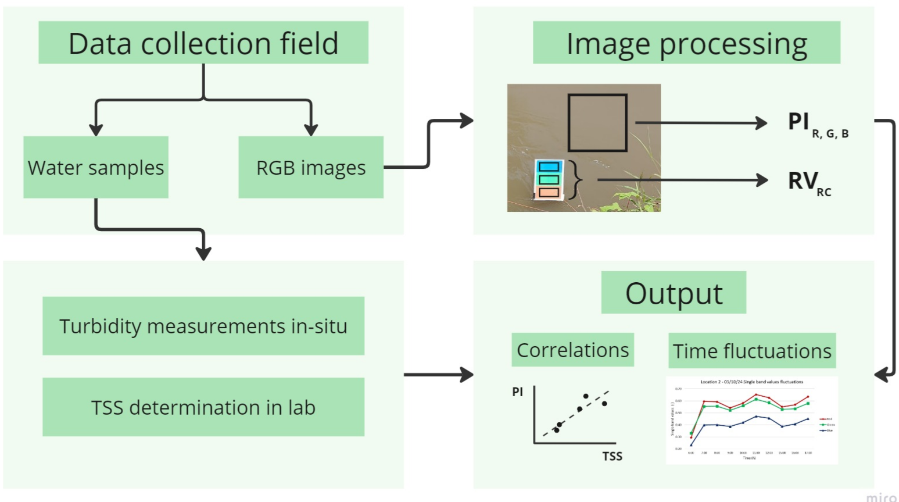

Figure 4.1: Schematisation of processing of RGB images

Image extraction

Photos were collected from water surfaces at three locations near weir constructions: location number 1, 2, and 3 (see Figure 3.1). Images were taken hourly during two time periods, 6:00-12:00 and 15:00-17:00, over two days. Two types of cameras were used, see Appendix A for specifications. In each photo, a section of the water surface was cropped to exclude reflections, turbulence, and other disturbances. Since it was not possible to crop the exact same area in every image at each location, the R, G, and B intensities for the cropped area were averaged based on the number of pixels selected. In Appendix B the crop coordinates of each image part and the code for deriving the RGB intensities is given.

Radiometric calibration

The radiometric calibration of the pixel values collected by the photo cameras was performed according to the methodology outlined by by Miglino et al. [14]. Since the distance between the water surface and the camera did not exceed 100 meters, atmospheric influences were assumed to be negligible [4]. A radiometric calibration panel with reference values Red (255, 0, 0), Blue (0, 0, 255) and Green (0, 255, 0) was used in the field and positioned on the water surface while collecting the photo image. The panel is used to eliminate the effect of the sun, environmental effects and the reflectance of the water. The radiometric calibration is performed according to Equation (4.2).

$$PI_{RC} = \left\{1, \frac{PI}{RV_{RC}}\right\} \tag{4.2}$$

Where PI represents the normalized pixel intensity value (Red, Green or Blue) of the cropped water surface and RV_{RC} denotes the normalized pixel intensity value (Red, Green or Blue) of the reference panel.

The pixel intensities values were normalized using Min-Max normalization, with RGB values ranging from 0 to 255 (4.3).

$$\text{Normalized value} = \frac{X - X_{\text{min}}}{X_{\text{max}} - X_{\text{min}}} = \frac{X}{X_{\text{max}}} = \frac{X}{255} \tag{4.3}$$

4.3 River sampling

To find an answer to the research question of what causes the high values of TSS in the Suan Mak River that lead to sediment accumulating in front of the hydraulic structures and silting up the reservoirs, two different approaches were used: synoptic TSS sampling and spatial sediment sampling. The locations of these samples have been carefully selected to determine the influence of both the national park and the agricultural areas. Therefore, we have chosen locations that are situated on the border with the national park, at a reservoir at the start of the agricultural area, or where two rivers converge.

Synoptic TSS sampling

Synoptic sampling is a method used to create a spatial overview of the water quality and sediment concentrations spread out over the river basin, and thereby identify the sources contributing to the high value of TSS in the Suan Mak River. The method involves collecting water samples from multiple points, typically upstream and downstream, including the main river and its tributaries, over a short period of time.
The locations that were chosen to collect the samples are as follows. The sample is taken at a hydraulic structure, for example, Location 2: The Kra Nae Weir, where the samples are collected upstream and/or downstream from a hydraulic structure near the CCTV cameras. The sample is taken at a location where a tributary connects with the Suan Mak River. Here, the sample is taken upstream in the main river, upstream in the tributary, and downstream in the main river. Samples are collected from reservoirs that are influenced either solely by agricultural activities or exclusively by the national park.
The samples were collected by throwing a bucket down from a higher point along the river or, when it was possible to come close enough to the river, with a bottle connected to an extendable stick. A turbidity measurement was performed on the spot. Then, the water samples were put in a 0.5 L plastic bottle and wrapped in aluminum foil to prevent light from getting in. The samples were then transported

to the lab to estimate the TSS through a Total Suspended Solids Measurement Experiment. A filter with a pore size of 1.2 μm was used.

Spatial sediment sampling

Obtaining sediment samples was challenging due to the high water levels in the rivers. Samples were collected at locations where access was feasible. Most of the samples were taken from the riverbanks, as it was difficult to reach near the middle of the riverbed because of the high flow. However, at smaller streams further upstream, it was possible on one occasion to collect a riverbed sample directly from the middle of the stream.
The samples were collected by digging up the top layer of soil and placing it in a Ziploc bag. The samples were taken to the soil lab, where they were dried at a temperature of 60 degrees and sieved into eight different grain sizes: $180,\mu$m, $150,\mu$m, $106,\mu$m, $75,\mu$m, $63,\mu$m, and $0,\mu$m.

Data processing

With the sediment- and TSS samples collected from the locations near the hydraulic constructions and reservoirs. We can make an estimation for sediment deposition. The boundary layer shear stress determines whether sediment remains in suspension or settles. When the shear stress is higher than a critical value, τ_c, the sediment can remain in motion. However, when $\tau_b < \tau_c$, the flow lacks the energy to carry the sediment, causing it to settle. For calculating deposition, we need to examine the relationship between τ_b and τ_c.
After that, a further examination can be conducted to determine the amount of sediment that settles inside the reservoirs. The following steps will be taken:

The settle velocity

First the settle velocity is being calculated.

$$V_s = \frac{(\rho_p - \rho_f) \cdot g \cdot d^2}{18 \cdot \mu} \tag{4.4}$$

where:

- V_s [m/s] is the settling velocity,
- ρ_p [kg/m^3] is the particle density,
- ρ_f [kg/m^3] is the fluid density,
- g [m/s^2] is the gravitational acceleration,
- d [m] is the particle diameter,
- μ [Pa□s] is the dynamic viscosity of water.

The settling distance (d_s)

By using the settling velocity, the settling distance d_s can be calculated that each particle can travel in the residence time:

$$d_s = V_s \times \text{residence time} \tag{4.5}$$

where:

- residence time [s]
- d_s [m] settling distance

Calculate Settling Efficiency

The settling efficiency is determined by the ratio of the settling distance to the water depth. If the settlings distance is less than the water depth the particle will not settle in the reservoir.

$$\text{Efficiency} = \left(\frac{\text{Settling distance}}{\text{Water depth}} \times 100\%\right) \tag{4.6}$$

Calculate the Mass of Settled TSS

Once we know the settling efficiency, we can calculate the amount of TSS that will settle:

$$\text{Settled TSS} = \text{TSS Concentration} \times \text{Q} \times \text{Settling efficiency} \tag{4.7}$$

where:

- TSS Concentration [mg/m^3]
- Q [m^3/s] Flow rate at location

Integrate Over Time

To find the TSS deposited over a given time period, integrate the settled TSS rate over the period.

4.4 Reservoir bathymetry

To provide an initial estimate of the reservoir storage volume, this section details the process of collecting bathymetry data, followed by the steps taken to process this data into a bathymetry map and the accompanying elevation-area-volume graph. This baseline will support ongoing research on sedimentation and volume changes within the reservoir.

Data collection

The water depth data for the bathymetry map of the reservoirs was collected using the Deeper Pro 2+, see Figure 4.2, an affordable commercial fish finder that also records water depth along with GPS coordinates, as shown in Figure 4.3. The device operates in conjunction with the 'Fish Deeper' mobile app, which could be installed on a smartphone or tablet. Within the app, users can customize scanning settings. For this experiment, the following settings were used: sensitivity at 20 percent, scanning angle at 20 degrees, and auto switch range enabled. In addition to sonar data, the app provides water depth, latitude and longitude. This raw bathymetry data can be exported in CSV format for further analysis. For the specifications of the Deeper Pro+2, see Appendix F .

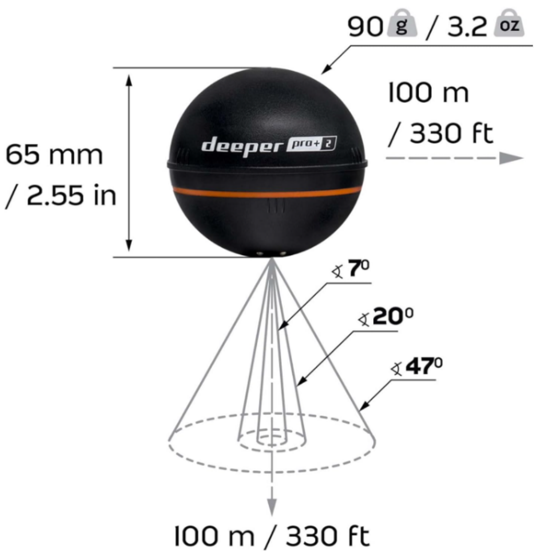

Figure 4.2: Deeper Pro 2+ [1]

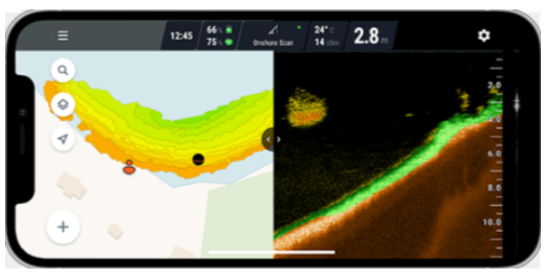

Figure 4.3: Fish Deeper app [2]

To measure the water depth, the Deeper Pro 2+ was attached to the side of a boat, which maintained a maximum speed of 4 km/h to minimize measurement disturbances. A custom mount, see Figure 4.4, was designed to keep the Deeper Pro 2+ consistently oriented downward, ensuring the signal transmitted vertically to the riverbed and minimizing the impact of waves on measurement accuracy. The mount was constructed from a foam board with a hole in which the Deeper Pro 2+ was securely placed. The foam board was held in place from the boat to maintain stability during the measurements. To prevent significant interpolation errors during data processing, contour lines were followed during data collection, based on the assumption that depth values along each contour line are similar. The routes for these contour lines were pre-planned using 'MyMaps.nl'. An example of the navigation lines can be seen in Figure 4.5, with the spacing between lines determined by the reservoir's size: 100 meters for Reservoir A, 25 meters for Reservoir B, and 50 meters for Reservoir C.
As water depth depends on water levels and this study focuses on the elevation of the bed, establishing a reference point is essential. This ensures that future measurements can be conducted and compared. For Reservoirs A and C, the elevation of the reference point was measured relative to Mean Sea Level, while for Reservoir B, a separate local reference point was used. Details regarding these reference points are provided in Appendix H.

Figure 4.4: Foam board with Deeper Pro 2+

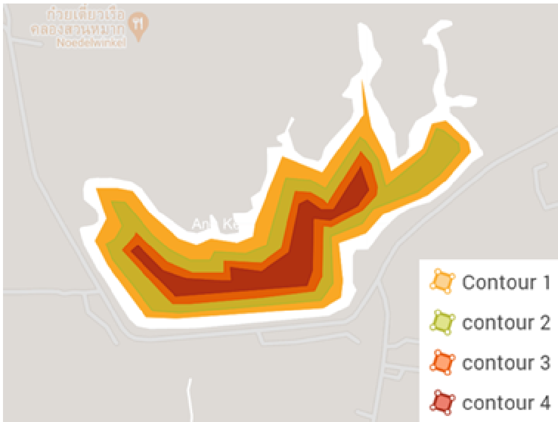

Figure 4.5: Route reservoir B in MyMaps

Data processing

The raw data obtained in the CSV file contained measurement errors caused by shallow water, fish interference, or poor connectivity. As a result, detectable errors were removed during the initial processing step. With 15 data points collected per second, the dataset contained a high volume of data. To improve the efficiency of the analysis, the data points were grouped by distance: 10 meters for Reservoir A, 5 meters for Reservoir B, and 2.5 meters for Reservoir C. For each group, the mean water depth and the average latitude and longitude coordinates were calculated. This grouping method enhanced the accuracy and efficiency of the interpolation process during subsequent data analysis. Figure 4.6 illuustrates the grouped data points for Reservoir B.

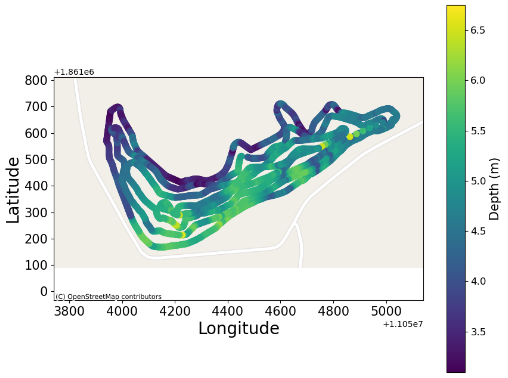

Figure 4.7: Sail Path Reservoir B

Figure 4.6: Cleaned datapoints Reservoir B

To create a bathymetry map from the collected data points, Inverse Distance Weighting (IDW) interpolation was applied with a power value of 2. In IDW interpolation, it is critical that the data points are evenly distributed in both the x- and y-directions to ensure consistent and accurate results. Uneven point density can lead to distortions, where closer points exert disproportionate influence. To address this, the data points were grouped by distance, maintaining a 1:10 ratio to ensure that for every point in one direction, there are 10 points in the other direction.
Using QGIS, a shapefile of the reservoir area was created, and the IDW plugin was applied to interpolate the data points within the reservoir boundaries. Since it was not possible to sail near the shorelines, see Figure 4.7 , it was assumed that the reservoir sides drop vertically without a slope and maintain the same depth as the outermost sailed contour line, as shown in Figure 4.8.

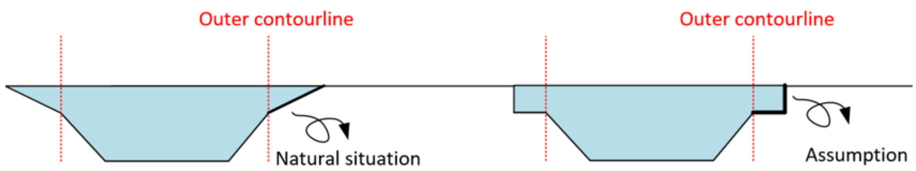

Figure 4.8: Assumption reservoir sides

After the interpolation, an Elevation-Area-Volume diagram was generated for the reservoirs. The surface area at each elevation was calculated using QGIS. First, contour lines were created at 0.5 m depth intervals using the contour plugin, and the corresponding surface areas were determined. The storage volume was then calculated using the trapezoidal formula:

$$V = \frac{(A_1 + A_2)}{2} \times (h_2 - h_1)$$

Construction drawings from 2012, provided by the Royal Irrigation Department of Thailand, were available for Reservoirs A and C. These drawings can be used for validation purposes.

5
Results

5.1 Sediment experiment results

in Figure 5.1 the results of the sediment experiment described in 4.1 are visualized.

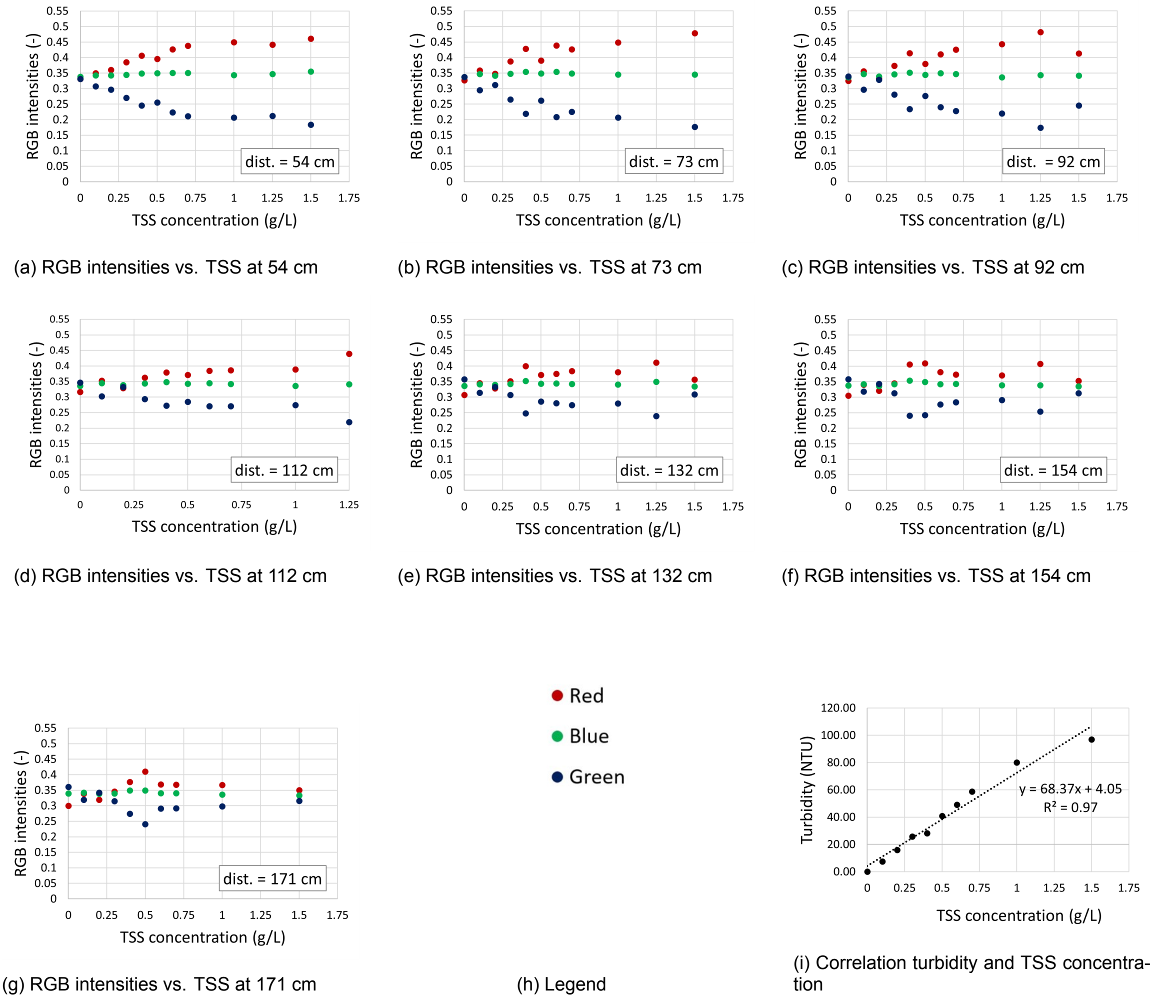

(a) RGB intensities vs. TSS at 54 cm

(b) RGB intensities vs. TSS at 73 cm

(c) RGB intensities vs. TSS at 92 cm

(d) RGB intensities vs. TSS at 112 cm

(e) RGB intensities vs. TSS at 132 cm

(f) RGB intensities vs. TSS at 154 cm

(g) RGB intensities vs. TSS at 171 cm

(h) Legend

(i) Correlation turbidity and TSS concentration

Figure 5.1: RGB intensity versus concentration at an angle of 0 degrees (vertical) for various distances.

Across all distances, RGB intensity generally increases with TSS concentration, with the red channel showing the most noticeable rise. The red intensity remains consistently higher than green and blue, and is less affected by distance.

At shorter distances (5.1a, 5.1b), the differences between the RGB intensities are more distinct. As distance increases (> 92 cm), the differences in RGB intensities diminish, though red still dominates. At even greater distances, all channels show less intensity variation, indicating reduced signal clarity. Beyond 1 g/L, RGB intensities tend to stabilize.

As SS concentration increases, it appears that particles scatter or absorb blue light more strongly compared to red light, leading to an increase in red intensity and a reduction in blue intensity.

5.2 RGB images constructions results

Location 1 – 05/10/24 and 06/10/24

In Figures 5.2 to 5.15 the fluctuations of the RGB intensities and turbidity over time are visualized for location 1, followed by the correlation plots of each intensity (Red, Green, Blue) with the TSS concentrations.

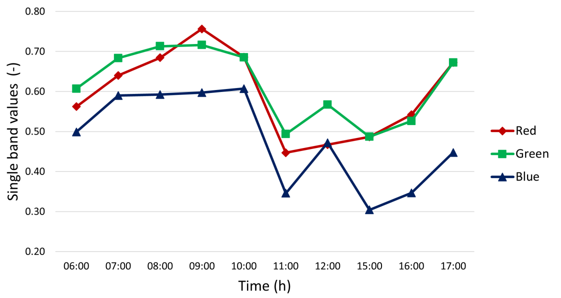

Figure 5.2: Location 1 - 05/10/24 Single band values over time

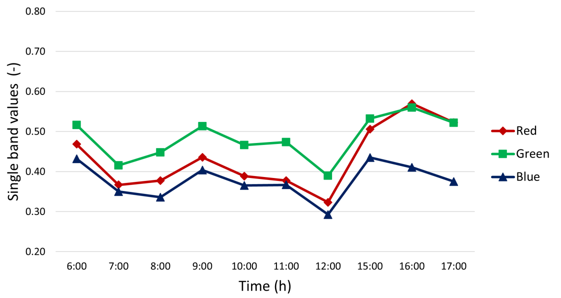

Figure 5.3: Location 1 - 06/10/24 Single band values over time

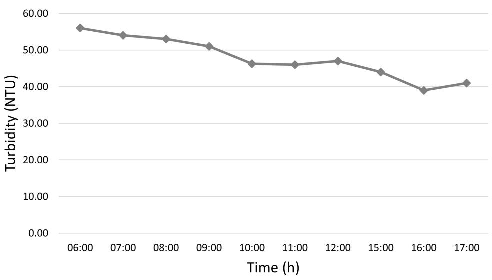

Figure 5.4: Location 1 - 05/10/24 Turbidity over time

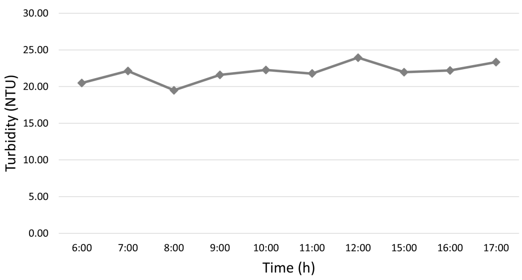

Figure 5.5: Location 1 - 06/10/24 Turbidity over time

Figure 5.6: Correlations of PI and TSS for Location 1 - 05/10/24 and 06/10/24

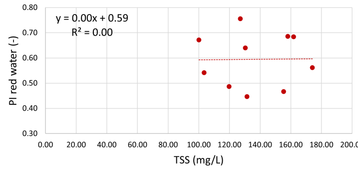

Figure 5.7: Location 1: PI red vs TSS 05/10/24

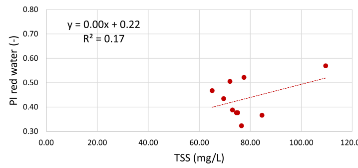

Figure 5.8: Location 1: PI red vs TSS 06/10/24

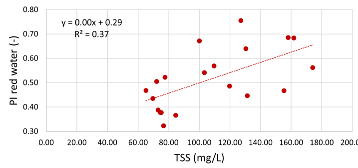

Figure 5.9: Location 1: PI red vs TSS 05/10/24 and 06/10/24

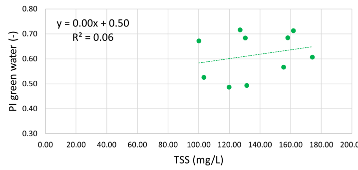

Figure 5.10: Location 1: PI green vs TSS 05/10/24

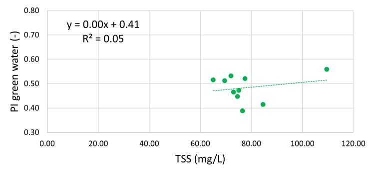

Figure 5.11: Location 1: PI green vs TSS 06/10/24

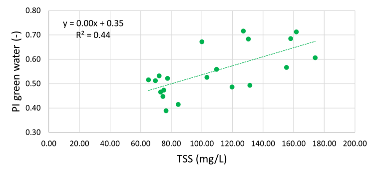

Figure 5.12: Location 1: PI green vs TSS 05/10/24 and 06/10/24

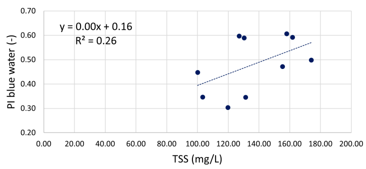

Figure 5.13: Location 1: PI blue vs TSS 05/10/24

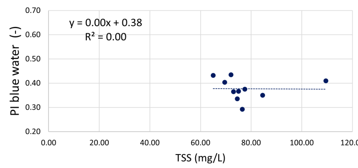

Figure 5.14: Location 1: PI blue vs TSS 06/10/24

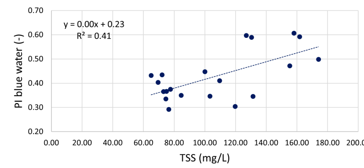

Figure 5.15: Location 1: PI blue vs TSS 05/10/24 and 06/10/24

The green band shows the highest pixel intensity values for this location and exhibits the best correlation with TSS looking at the datapoints combined over 05/10/24 and 06/10/24, making it the most reliable option for detecting sediment at this location. The red and blue band have slightly weaker correlations, indicating limited effectiveness for sediment detection. Although the green band suggests some detectability of sediment, the low R^2 values imply that this correlation is not strong.
Temporal variability is evident in the pixel intensity (PI) values over time. The fluctuations in PI throughout the day indicate this, with peaks occurring between 10:00 and 14:00. This is likely due to sunlight interference, which affects sediment detection accuracy. Meanwhile, turbidity remains stable, indicating consistent sediment conditions.

Location 2 – 03/10/24 and 04/10/24

In Appendix D.1, the results for location 2 are visualized. The RGB intensity values show variability throughout the day, with observable fluctuations in all bands on both 03/10/24 and 04/10/24. The pixel intensity values of the green band generally maintain the highest levels, while the red band exhibits some fluctuations, and the blue band remains relatively low. On 03/10/24, all bands display a moderate negative correlation with TSS, suggesting that higher sediment concentrations may lead to lower pixel intensity values. However, the overall predictive power remains weak across all bands, even when the data points from both days are combined.
Turbidity measurements show a steady decline throughout the day, which aligns with a decrease in TSS. In contrast, the RGB intensities do not show a clear trend over the day.
Again the midday peaks in pixel intensity values indicate the influence of sunlight on the RGB bands, which interferes with the accuracy of sediment detection.

Location 3 – 07/10/24 and 08/10/24

For Location 3, the results can be found in Appendix D.2. Across both days (07/10/24 and 08/10/24), the correlations between RGB intensity values and TSS are very weak. This indicates that sediment detection using RGB is not reliable at this location under the observed conditions. While the green

band shows slightly better correlations with TSS compared to the red and blue bands, the overall effectiveness remains limited. The RGB intensities show fluctuations throughout the day, but these do not correlate well with changes in sediment concentration. No clear trends can be observed in pixel intensity values over time.
Again peaks during midday in intensities suggest that sunlight is influencing the RGB values, potentially masking the sediment signal.
The generally low sediment concentrations at this location make it challenging to detect sediment using RGB intensities, as insufficient variation in TSS limits the potential for strong correlations with band values.

Validation of RGB images results

The correlation between TSS and turbidity values obtained is quite strong, as can be seen in 5.16. This strong correlation indicates that the turbidity trends observed throughout the day are consistent across different locations for TSS, suggesting that turbidity is a reliable proxy for TSS in the context of these measurements.
Furthermore, Figure 5.17 shows that the average light intensity is highest around 11:00 and 12:00, coinciding with peaks in the RGB intensity values for each location. This suggests that the increased light intensity during these hours may significantly interfere with the data captured in the RGB images, underscoring the importance of considering light conditions when analyzing RGB image data.

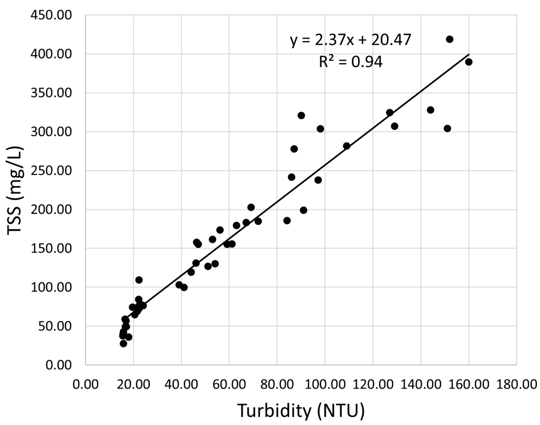

Figure 5.16: Correlation between Turbidity and TSS

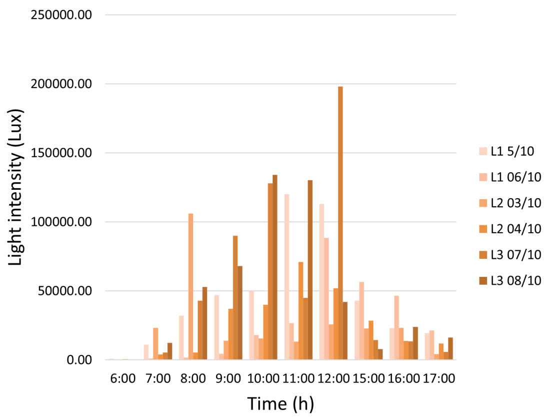

Figure 5.17: Light intensity fluctuation during the day

5.3 River sampling results

Below, two diagrams are visible for the synoptic TSS sampling. The diagram in Figure 5.21 gives an overview of the sample results taken during a time period of 7 days of dry weather. In Figure 5.22, the results of a rainy period of 2 days are shown. Additionally, a graph is visible for the sediment sampling.

Filters TSS lab experiment

During the TSS experiment in the lab, different types of TSS were visible on the filters, indicating variations in the composition and particle sizes among the samples. Some filters showed a very uniform and smooth residue, where the TSS appeared very fine, while other filters contained larger grain sizes. The variation of residue samples is shown in Figures 5.18, 5.19, and 5.20.

Figure 5.18: Residue of TSS on a filter from sample Location 8 upstream 2. This is a side river.

Figure 5.19: Residue of TSS on a filter from sample Location 7 upstream 1. This is a main river.

Figure 5.20: Residue of TSS on a filter from sample Loc 8 upstream 1 river. This is a main river.

Dry weather 5/10/2024 till 11/10/2024

The graph indicates that TSS values in the main river start relatively low, around 9 mg/L, at the boundaries of the National Park. As the river flows further, the TSS values increases, peaking at 90 mg/L. This is due the inflow of tributary with a concentration of 111 mg/L.

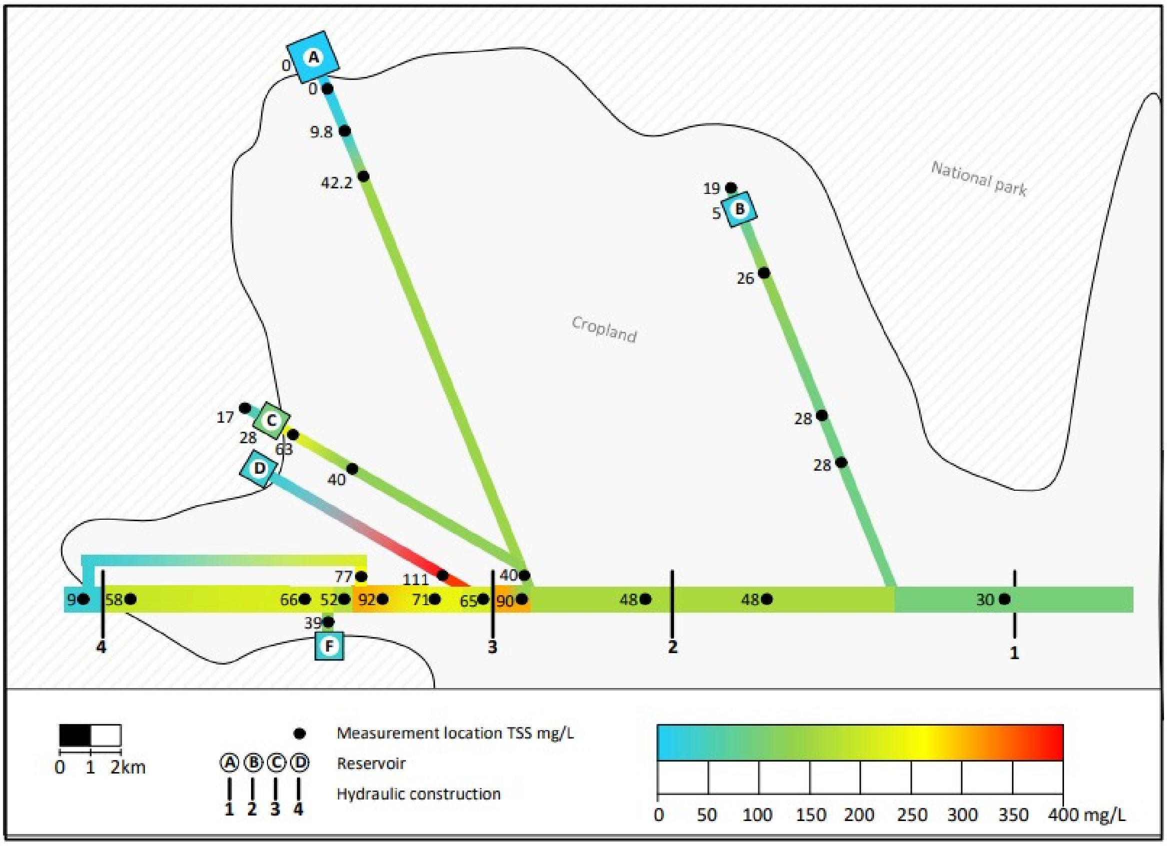

Figure 5.21: A schematic overview of the TSS values during a dry event over a 7-day period in the research area

Rain event 3/10/2024 and 4/10/2024

Figure 5.22 shows a schematic overview of the water sampling area during a rain event. The river starts relatively low upstream on the left side near the national area. The value then increases to a maximum of 359 mg/L.

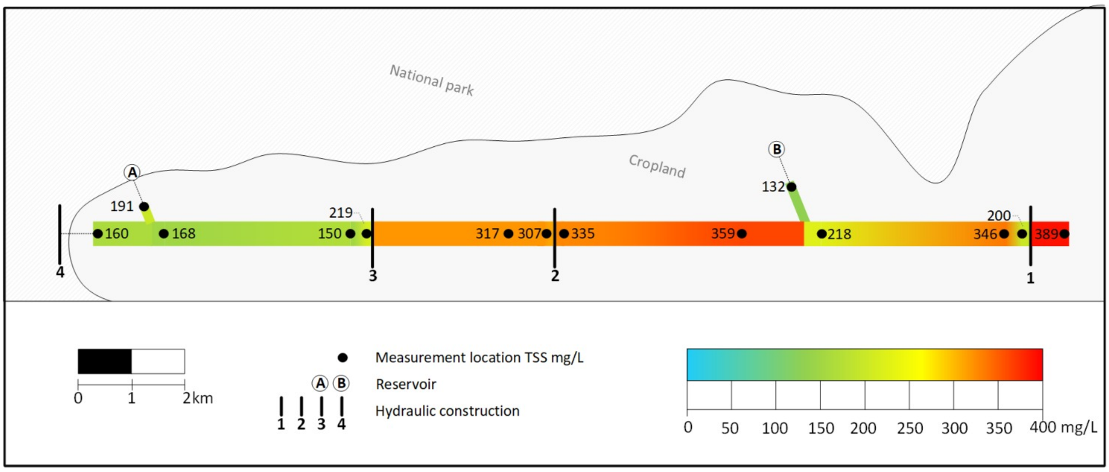

Figure 5.22: A schematic overview of the TSS values during a rain event over a 2-day period in the research area.

5.4 Spatial sediment sampling

The results of the spatial sediment sampling are visualized in Figure 5.23. Most of the data points cluster near the sand-rich region (bottom side of the triangle), indicating that the majority of the soil samples contain a high percentage of sand. The points are far from the grind (gravel) axis, indicating that the soils have very low amounts of gravel or coarse particles. Only a few samples show somewhat higher percentages of silt. This went against our expectations, as it was thought that there would be a high amount of TSS.

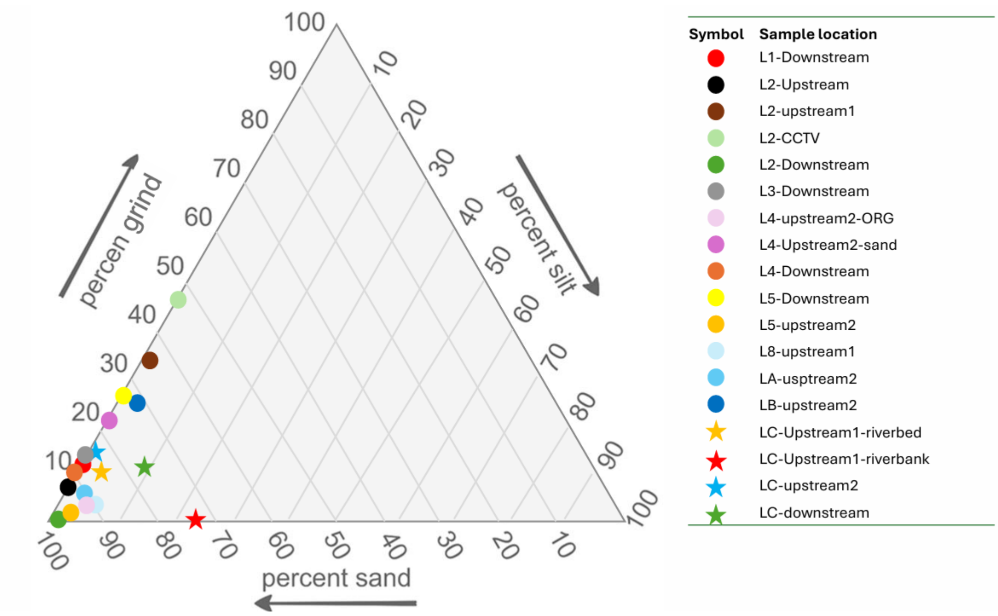

Figure 5.23: A graph showing the ratio percentages of grind, sand, and silt within the soil samples taken at different locations in the research area.

This can be explained as follows. While the flow force is capable of carrying all grain sizes along the river, as shown in Figure 5.24, almost all particles are in suspension. However, what the Shield graph does not show is that some particles have a higher chance of settling than others. For example, at

Location 1, a particle of 2.36 mm has a 100% chance of settling within the reservoir [E.1], while a particle of $63, \mu$m has only an 11% chance [E.1]. This could explain why a lot of sand is found at the reservoirs at the hydraulic structures.
However, when we look at the settling efficiency of the particles in Reservoir A, which has a much larger volume than the river, it can be seen that all particles have a settling efficiency of 100% [E.2]. When calculating the volume of the settled sediment, we arrive at a total of 16,000 kg/year. It should be noted that a concentration of 19 mg/L was also used for particles with a grain size greater than 0.001 mm, even though these were not present in the suspended sample.

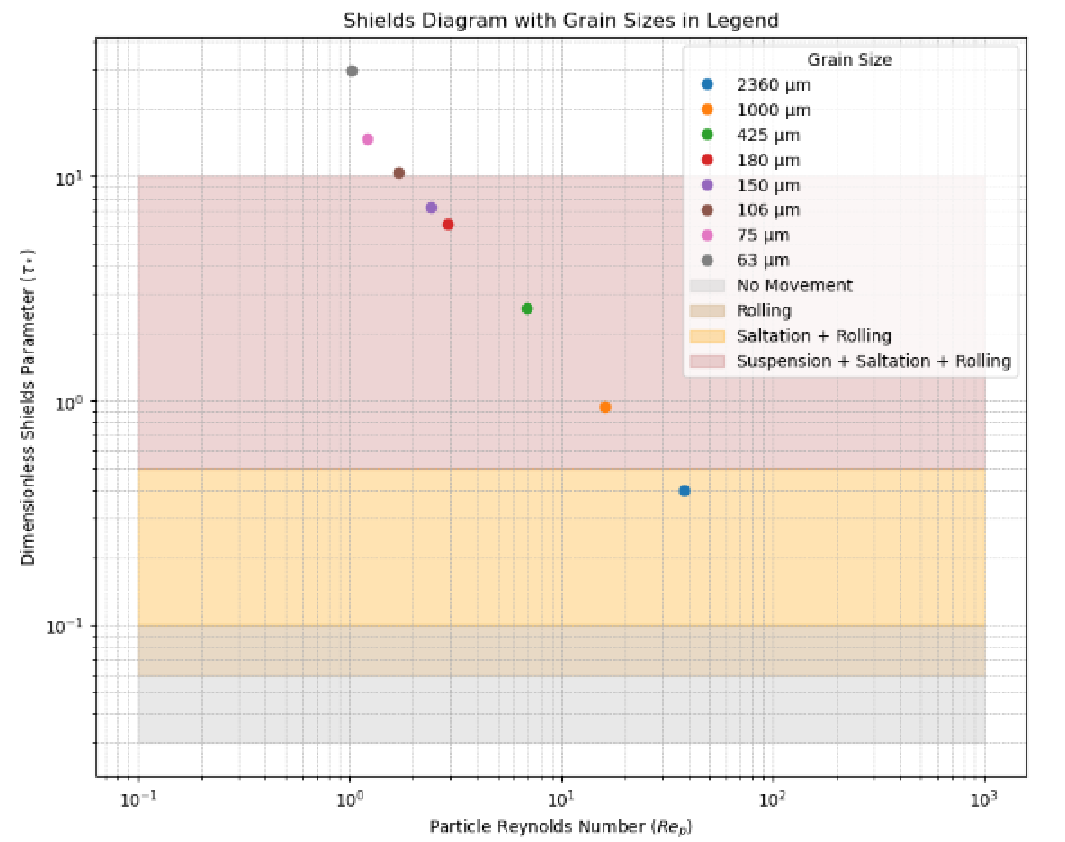

Figure 5.24: Shields Diagram illustrating the relationship between the particle Reynolds number (Re_p) and the dimensionless Shields parameter (τ_*) for various sediment particles in water flow. Blue points represent calculated values for particles of different sizes and densities, showing their propensity for movement under the given shear stress.

5.5 Reservoir bathymetry

Bathymetry maps and corresponding Elevation-Storage-Area Diagrams were generated for Reservoir A, B, and C. Additionally, cross-sections were created for each reservoir. For Reservoir A, the depth profiles from the 2012 construction drawing were incorporated into the cross-sections for comparison.

Reservoir A

Figure 5.25 shows the bathymetry map of Reservoir A and Figure 5.26 depicts the corresponding Elevation-Area-Volume Diagram.

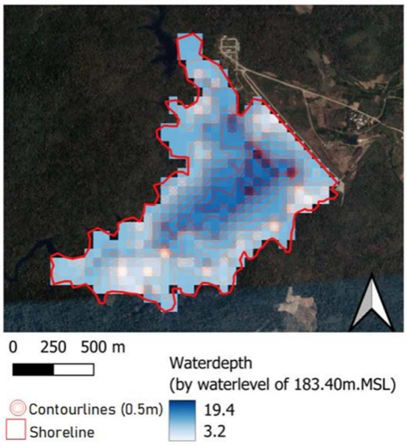

Figure 5.25: Bathymetry map Reservoir A

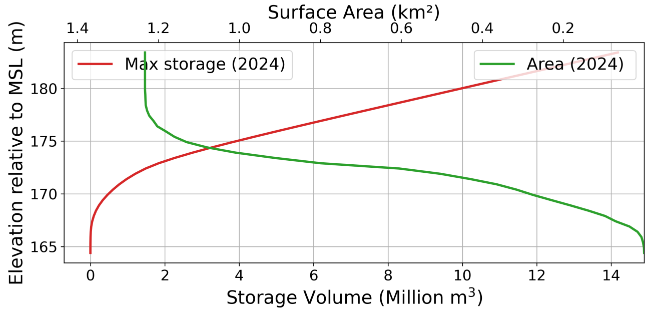

Figure 5.26: Elevation-Area-Volume Diagram Reservoir A

Subsequently, the created Elevation-Volume-Area diagram of 2024 was compared to the diagram based on the construction drawings from 2012.

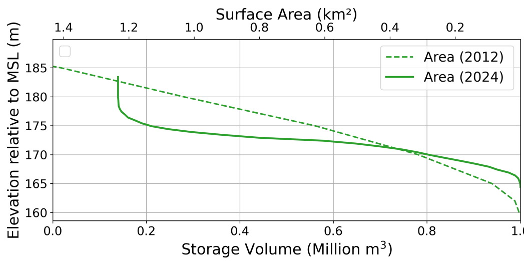

Figure 5.27: Elevation-Area Diagram of Reservoir A: 2012 & 2024

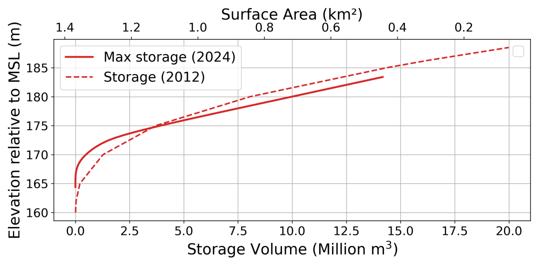

Figure 5.28: Elevation-Volume Diagram of Reservoir A: 2012 & 2024

Several cross-sections of the reservoir were created to get a first impression of how the reservoir bed profile has changed in comparison to the construction drawings. The exact locations of these cross-sections can be found in Appendix G.

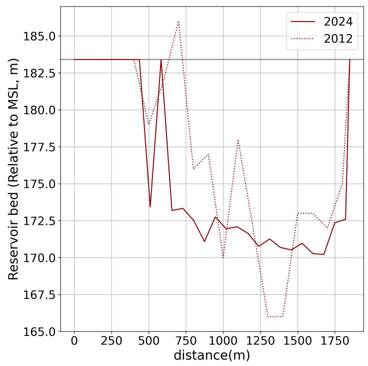

Figure 5.29: Cross section 1 - Reservoir A

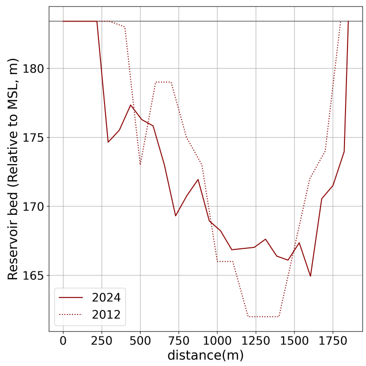

Figure 5.30: Cross section 2 - Reservoir A

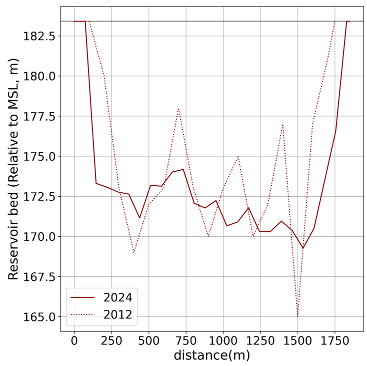

Figure 5.31: Cross section 3 - Reservoir A

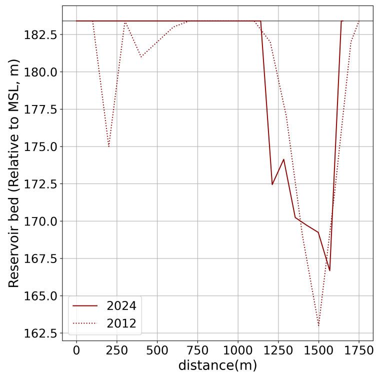

Figure 5.32: Cross section 4 - Reservoir A

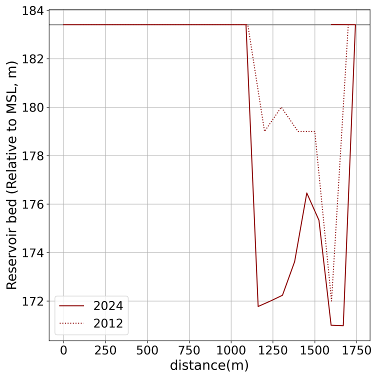

Figure 5.33: Cross section 5 - Reservoir A

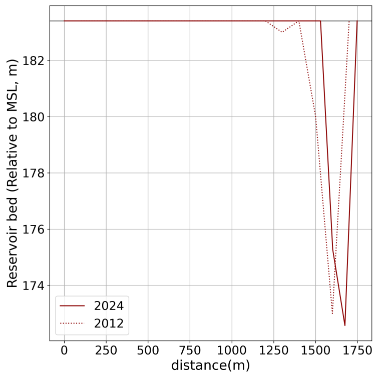

Figure 5.34: Cross section 6 - Reservoir A

Reservoir B

Figure 5.35 shows the bathymetry map of Reservoir B, and Figure 5.36 depicts the corresponding Elevation-Storage-Area Diagram.

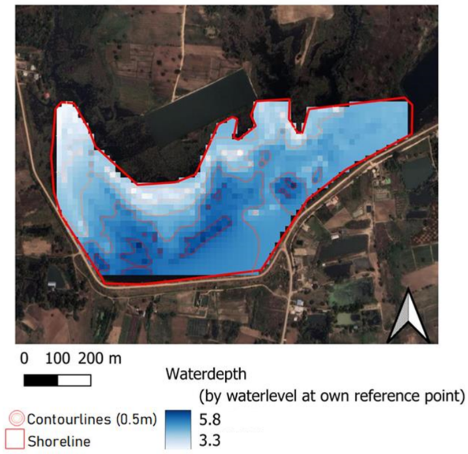

Figure 5.35: Bathymetry map Reservoir B

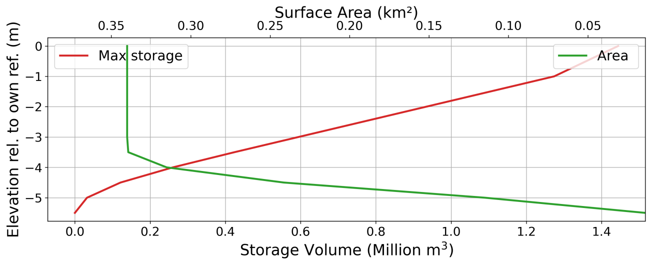

Figure 5.36: Elevation-Volume-Area Diagram of Reservoir B: 2024

Several cross-sections of the reservoir were created to get a first impression of the reservoir bed profile. The exact locations of these cross-sections can be found in Appendix G.

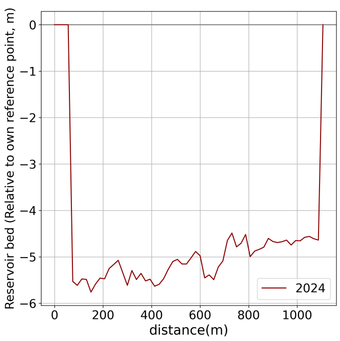

Figure 5.37: Cross section 1 - Reservoir B

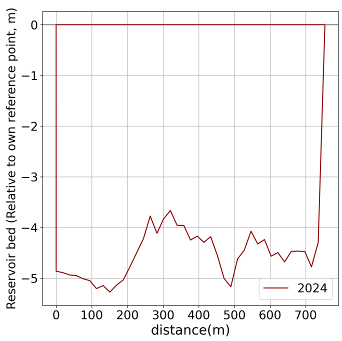

Figure 5.38: Cross section 2 - Reservoir B

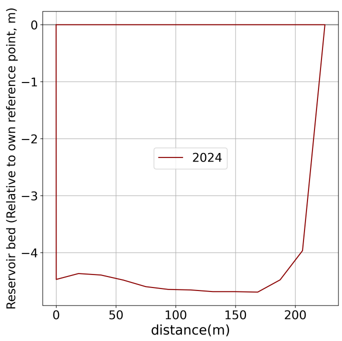

Figure 5.39: Cross section 3 - Reservoir B

Reservoir C

Figure 5.40 shows the bathymetry map of Reservoir C, Figure 5.41 depicts the corresponding Elevation-Area-Volume Diagram.

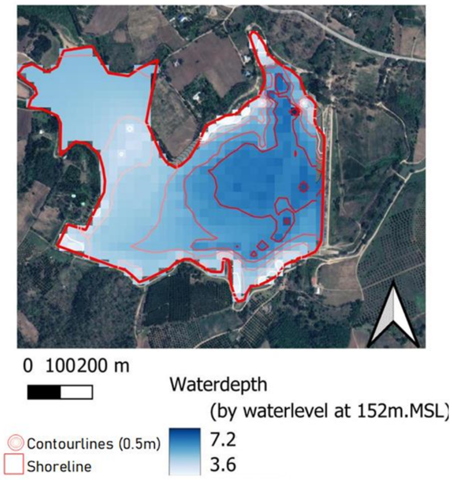

Figure 5.40: Bathymetry map Reservoir C

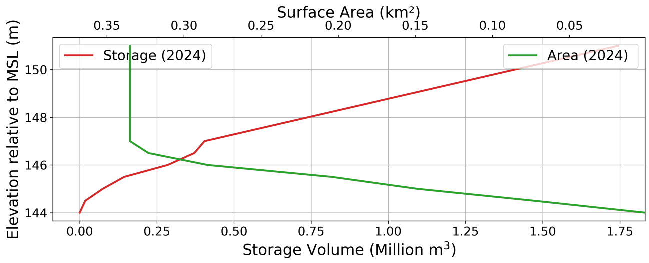

Figure 5.41: Elevation-Storage-Area Diagram Reservoir C

Subsequently, the created Elevation-Volume-Area diagram of 2024 was compared to the diagram based on the construction drawings from 2012.

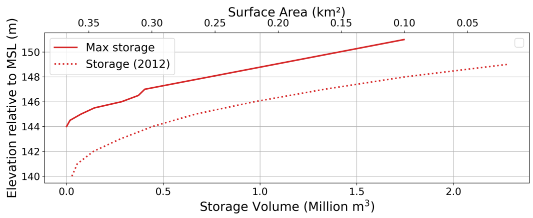

Figure 5.42: Elevation-Volume Diagram of Reservoir C: 2012 & 2024

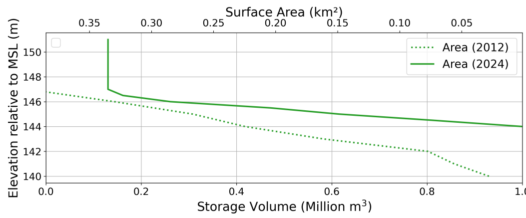

Figure 5.43: Elevation-Area Diagram of Reservoir C: 2012 & 2024

Several cross-sections of the reservoir were created to get a first impression of the reservoir bed profile. The exact locations of the cross-sections can be found in Appendix G.

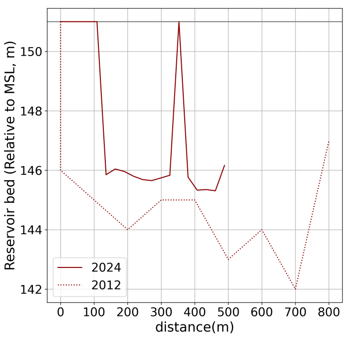

Figure 5.44: Cross section 1 - Reservoir C

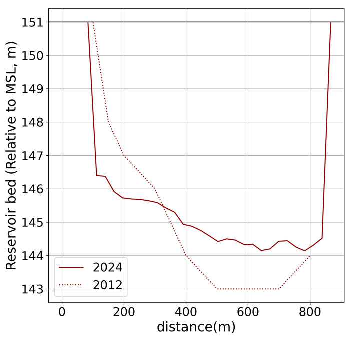

Figure 5.45: Cross section 2 - Reservoir C

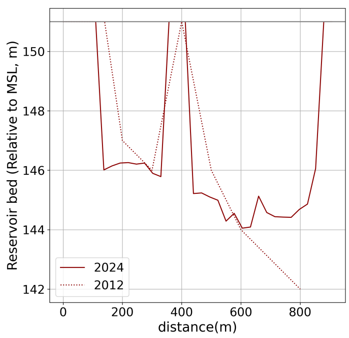

Figure 5.46: Cross section 3 - Reservoir C

6

Discussion & Recommendations

The discussion and recommendations chapter is divided into three sections: RGB image collection, bathymetry measurements, and river sampling.

6.1 RGB data collection

Requirements for RGB trends detectability

Camera position optimalization

To ensure clarity in detecting different RGB intensities, position the camera as close to the water surface as possible, ideally within 100 cm, as greater distances (over 92 cm) produce inconsistent trends (5.1). A vertical angle (0 degrees) is recommended, as this minimizes reflectance disturbances in the image based on fieldwork observations.

A possibility for obtaining this small distance would be implementing floating or amphibious drones equipped with cameras and sensors to capture water surface data. For instance, research by Cheng et al. (2021) [3] describes a six-rotor floating UAV designed for monitoring water quality. This drone captures consistent, close-range images and data from the water surface, which can help reduce interference from ambient light and environmental disturbances.

Requirements for Suspended Sediment (SS) concentrations

For low TSS concentrations and minimal variability in TSS concentrations, detecting differences in the RGB intensity bands becomes challenging. Therefore, a minimum concentration of 0.3 g/L is recommended to effectively distinguish differences in RGB intensities, as shown in Figure 5.1. In the field, the maximum range of TSS detected was approximately 0.24 g/L, which resulted in still a weak correlation between TSS and pixel intensity. However, in the sediment experiment, where TSS ranged from 0.3 to 1.5 g/L, a clear trend was observed.

A difference of approximately 1.2 g/L in the field should provide a better correlation between TSS and pixel intensity. Therefore, it is recommended to focus on collecting time series of RGB images during periods with significant fluctuations in TSS concentrations, such as after rain events.

Given the limitations of RGB images for detecting TSS due to minimum concentration and variability, advanced imaging technologies like photo-spectral cameras may be more effective. These cameras capture a broader range of wavelengths beyond the visible spectrum. As highlighted by Nayak et al. (2023) [15], photo-spectral cameras, especially those using NIR (Near-Infrared), can provide more detailed data for detecting sediment particles. This allows for more precise TSS detection, particularly when sediment concentration and variability are low.

Effect of light intensity fluctuations

The effect of light interferes with the RGB intensities derived during midday, from 10.00 to 14.00. The use of the reference colors unfortunately does not filter out this light intensity fluctuation, therefore another way to get rid of this interference must be implemented in further research.

To enhance the accuracy of TSS concentration estimates from RGB images, under varying ambient conditions, a protocol similar to that developed by Leeuw and Boss (2018) [11] could be adapted. Their method, designed for smartphone-based estimations of SSC, provides a way to account for ambient light effects. This approach involves capturing a series of images of the water surface, sky, and a grey reference standard to correct for ambient light effects. Using these images, remote sensing reflectance can be calculated (see Equation 6.1), which helps normalize the RGB values.

$$R_{rs} = \frac{L_t - \rho L_s}{\pi \cdot R_{ref} \cdot L_c} \tag{6.1}$$

with R_{rs} the remote sensing reflectance, L_t the radiance leaving the water surface, L_s the sky radiance, R_{ref} the reflectance of a standard reference, L_c radiance leaving the reference standard and ρ the sea surface reflectance factor.
Another way to reduce the effect of fluctuating ambient light, would be by establishing controlled or artificial light conditions, they help reduce the effects of ambient light variability that can distort reflectance readings. Studies, such as those by Liu & Zhang (2019) [12], have shown that controlled lighting minimizes interference from changing sunlight or weather conditions, leading to more consistent reflectance data that closely correlates with SSC levels.

6.2 Reservoir bathymetry

Recommendations for bathymetry measurements

This study provided valuable insights into conducting depth measurements using the Deeper Pro+ 2. It can be concluded that a custom-made construction, consisting of a foam board with a hole for the depth sensor, is an effective and cost-efficient method for minimizing wave disturbances and ensuring the depth sensor remains downward-facing. This setup is recommended for future depth measurements. Additionally, the generated bathymetry maps and their corresponding Elevation-Volume-Area diagrams can serve as preliminary estimations of reservoir storage capacity. However, to improve the accuracy of these estimations, the following recommendations are proposed:

1. Navigating Contour Lines: When mapping contour lines, it is recommended to navigate the outermost contour line as closely as possible to the reservoirs outer bank. This approach provides valuable information about the depth near the shoreline and contributes to a more accurate estimation of the reservoir's total surface area.
2. Gaining Additional Depth Profile Data: To gather more detailed information about the depth profile between the shoreline and the outer contour line, it is suggested to use a manual depth device that can accurately measure shallow waters. This method would enable more reliable assumptions about the depth profile than the simplified square profile assumption used in this study.
3. Exploring Advanced Interpolation Techniques:To improve the accuracy of depth data processing, alternative interpolation techniques should be considered. For instance, geostatistical methods such as Kriging, which consider spatial autocorrelation, could provide a more accurate representation.
4. Alternative Sailing Routes: Navigating contour lines may not always be the most effective method for depth measurements. Therefore, exploring alternative sailing routes should be considered.

Discussion for Bathymetry measurements

During the measurements, it was not always possible to navigate closely along the shorelines of the reservoir. This was due to the presence of dense vegetation, people fishing near the outer banks, and

areas too shallow for the Deeper Pro+2 to measure accurately. Consequently, limited information was obtained about the depth near the shorelines, as well as the total surface area and the shape of the reservoirs.
In processing the data, a square depth profile was assumed between the outermost contour line and the shoreline. For large and deep reservoirs such as Reservoir A, which has a maximum depth of 20 meters and a surface area of 1.2 km², this assumption significantly impacts storage capacity calculations. The outermost contour line encompasses a large storage volume, the choice between the assumption of a square profile or a sloped profile (45-degree angle) could result in a difference of approximately 4 million cubic meters in estimated water storage for Reservoir A at the measured water level.
Additionally, IDW interpolation was used as the interpolation method for processing the data. However, IDW is less suitable for unevenly distributed data along the x- and y-axes because it only considers distance without accounting for spatial relationships. Furthermore, IDW tends to over-smooth data, as it does not account for clustering or directional patterns, which can reduce the accuracy of the bathymetric map.

6.3 River sampling

The application of synoptic sampling has shown that, during rainfall, the agricultural area has a significant influence on the increase in TSS concentration in the Khlong Suan Mak River. When comparing dry days and rainy days, the national park area shows relatively low values in both cases and therefore has little influence on the sediment concentration downstream. It is possible, however, that TSS has had time to settle before Construction 4, resulting in a low value measured in front of the weir. It should also be noted that sediment sizes from 1.06×10^{-4}m till 2.36×10^{-3} m at Locations 1 and 2 have a 100% chance of settling and accumulating in front of these structures. This means that this sediment is trapped behind the weirs and cannot accumulate at the next structure. Nevertheless, the dams up to Location 2 are visibly filled with sand. This sand should be collected in the segments between the structures.
The dominant grain size of sediment found in the dams is 4.25×10^{-4}m; however, according to Table 5.23, this is the main contributor to the silting up of the dams. This conclusion is based only on sediment found at the side of the reservoir. Research indicates that sediment settles in layers, which means that the composition of sediment may differ in the middle of the reservoir [7]. This could be confirmed in a follow-up study by taking a sample from the center of the reservoir.
Additionally, calculations for Reservoir A indicate a sediment build-up of 16,159.0 m³ per year. This is a low number compared to the bathymetry measurement, which showed a storage difference of 4 million m³. It should also be noted that, in calculating settled particles, the TSS concentration was used for all particle sizes. From Figure 5.24, we can conclude that particles with a grain size of 2.36 mm are not present in this layer. Therefore, it is possible that the concentration of particles outside the TSS range could be higher or lower in the water, which could result in a different calculation. Additionally, a portion of the reservoir was not included in the bathymetry measurements due to vegetation obstructions, which may have introduced uncertainty in the measurement of changes in reservoir storage.

7 Conclusion

RGB images constructions

Based on the findings, RGB imaging for sediment detection has limitations, especially under field conditions with low and minimally variable TSS concentrations. The correlation between RGB intensity values and TSS is weak, and a minimum variability of 1.2 g/L in TSS is recommended for more reliable detection. No specific RGB band emerges as the most consistent indicator, and environmental factors, particularly light intensity fluctuations, must be considered, as they significantly impact detection accuracy.
To improve sediment detection, it is recommended to position the camera within 100 cm of the water surface and at a vertical angle (0 degrees) to reduce reflectance disturbances. Using floating drones for close-range imaging can help minimize interference from environmental factors.
For more precise TSS detection, photo-spectral cameras, which capture a broader spectrum including NIR (Near-Infrared), may provide better accuracy, particularly in conditions with low sediment concentration. Additionally, turbidity measurements, which show a strong correlation with TSS, can serve as a reliable proxy for estimating sediment concentrations in various conditions.
In addition, to further investigate the TSS concentration in the study area, it is recommended to do this at location 2. At this location, the concentration fluctuates the most, increasing the likelihood of detecting differences in concentrations. It is also advisable to conduct measurements during early mornings and afternoon when the light intensity is lower, which minimizes reflections from the water surface.
In conclusion, while RGB imagery provides valuable insights, it is important to account for environmental variables and camera positioning to improve detection. Future research could focus on combining RGB data with other imaging technologies, such as photo-spectral cameras or turbidity measurements, to enhance sediment detection accuracy under varying field conditions.

Reservoir Bathymetry

The Elevation-Volume-Area diagrams provide a preliminary estimation of the reservoirs' storage volume . The storage volumes measured on the observation day are summarized in Table 7.1, along with any available previous measurements. From these results, it can be concluded that the measurements fall within the same range as the initial observations, providing a reasonable estimate of storage volume. However, these measurements do not provide insights into the deposited sediment. To improve measurement accuracy, it is necessary to navigate closer to the shorelines of the reservoirs.

Table 7.1: Storage volume at different water levels

Reservoir	At a water level of	Year	Storage Volume
A	183 m MSL	2012	11 million m^3
A	183 m MSL	2024	14 million m^3
B	0 m relative to reference point	2012	No data
B	0 m relative to reference point	2024	1.4 million m^3
C	152 m MSL	2012	1.8 million m^3
C	152 m MSL	2024	0.8 million m^3

Cross-section analyses indicate that the lowest point in Reservoir A has risen by 5 meters. This observation suggests that sediment deposition has occurred, resulting in a significantly smoother reservoir bed. This provides evidence of sedimentation and its impact on the reservoir's morphology.

Appendices

A

Camera specifications

Table A.1: Camera Specifications

Type of camera	iPhone 12 Mini	OnePlus 10T 5G
Resolution	3024 x 4032 pixels (12 MP)	3072 x 4096 pixels (12.6 MP)
Bit Depth	32 bits	24 bits
Aperture (F-stop)	f/1.6	f/1.8
Shutter Speed	1/121 second	Not specified
Focal Length	26 mm	5.59 mm

Table A.2: GPS Coordinates of RGB Image collection per location

Location number	**GPS Latitude**	**GPS Longitude**	**GPS Altitude**
1	16° 26’ 57.33”	99° 25’ 22.54”	90.77 meters
2	16° 25’ 11.21”	99° 22’ 37.44”	102.31 meters
3	16° 24’ 49.79”	99° 21’ 15.87”	108.41 meters

B

Crop coordinates RGB images

B.1 Crop coordinates sediment experiment

Table B.1: Crop coordinates of sediment experiment for angle of 0 degrees over various relative distances

Angle	Relative Distance	Left	Upper	Right	Lower	Pixel Count Cropped
0	54	750	1250	1850	1800	605000
0	73	1160	1250	1850	1800	379500
0	92	1360	1300	1850	1800	245000
0	112	1600	1300	1850	1800	125000
0	132	1700	1400	1900	1700	60000
0	151	1800	1400	1900	1700	30000
0	171	1830	1400	1900	1700	21000

B.2 Crop coordinates fieldwork

Table B.2: Crop coordinates for fieldwork images - part 1

Image num.	Image Title	Left Water	Upper Water	Right Water	Lower Water
1	3_06.00_07.10_16.53_63_3.71_refl.turb.shad	2000	0	3072	1300
2	3_07.00_07.10_15.46_5300_3.67_refl.shad	2000	0	3072	1300
3	3_08.00_07.10_22.53_43000_3.61_refl.sun	2000	0	3072	1300
4	3_09.00_07.10_15.66_90000_3.63_refl.sun	2100	0	3072	1300
5	3_10.00_07.10_16.40_128000_3.62_refl.sun	1600	0	1900	1000
6	3_11.00_07.10_15.72_45000_3.61_refl.shad	1600	0	1900	1000
7	3_12.00_07.10_16.97_198000_3.61_refl.sun	1500	0	2300	1000
8	3_15.00_07.10_16.80_14500_3.66_refl.shad	2300	0	3072	500
9	3_16.00_07.10_15.61_13500_3.68_refl.shad	2600	0	3072	500
10	3_17.00_07.10_17.91_5900_3.65_shad	2000	0	3072	1000
11	3_6.00_08.10_13.79_120_3.88_shad	1600	0	3024	800
12	3_7.00_08.10_14.93_12315_3.75_refl.shad	1050	200	1200	800
13	3_8.00_08.10_15.06_52901_3.88_refl.turb	2400	1250	3024	1500
14	3_9.00_08.10_16.04_68000_3.94_refl.shad	2000	900	3024	1300
15	3_10.00_08.10_13.31_134124_4.02_refl.sun	2250	1500	3024	1700
16	3_11.00_08.10_11.52_130264_3.98_refl.sun	2500	1200	3024	1400
17	3_12.00_08.10_13.92_42000_3.91_refl.turb.sun	1000	800	1200	1600
18	3_15.00_08.10_14.00_7800_3.89_refl.turb	1300	0	1450	1750
19	3_16.00_08.10_14.62_23900_3.91_shad	2000	1300	3024	1850
20	3_17.00_08.10_12.73_16186_3.90_refl.turb.shad	2200	0	3024	900
21	1_06.00_05.10_56_860_5.17_shad	0	0	1500	850
22	1_07.00_05.10_54_10900_5.17_shad	0	0	1500	1350
23	1_08.00_05.10_53_32000_nan_shad	0	0	1500	1700
24	1_09.00_05.10_51_47000_5.25_sun	0	200	1500	1900
25	1_10.00_05.10_46.28_50000_5.25_refl.turb	0	200	1200	1200
26	1_11.00_05.10_46_120000_5.27_refl.sun	1300	1700	1800	1000
27	1_12.00_05.10_47_113000_nan_sun	1300	1770	2000	1900
28	1_15.00_05.10_44_43000_5.3_refl.shad	1300	2000	1700	1600
29	1_16.00_05.10_39_23000_5.33_refl.turb.shad	1150	1800	1450	1500
30	1_17.00_05.10_41_19300_5.37_sun	2200	800	3600	1400
31	1_6.00_06.10_20.48_297_5.44_shad	0	0	1400	1600
32	1_7.00_06.10_22.12_1091_5.5_shad	0	1400	1200	1700
33	1_8.00_06.10_19.49_1673_5.53_shad	1300	1200	2300	1900
34	1_9.00_06.10_19.64_4300_5.56_refl.sun	1500	1200	2200	1200
35	1_10.00_06.10_21.64_3200_5.56_shad	1000	0	2100	1400
36	1_11.00_06.10_20.53_3100_5.58_shad	1100	0	2000	1200
37	1_12.00_06.10_20.24_9500_5.58_shad	1500	0	2000	1200
38	1_15.00_06.10_20.03_4500_5.56_shad	0	0	2100	1500
39	1_16.00_06.10_19.27_3400_5.58_shad	0	200	2200	1500
40	1_17.00_06.10_19.58_2200_5.58_shad	0	0	2200	1500
41	2_6.00_4.10_152_700_5.02_turb.shad.jpg	1400	500	1600	900
42	2_7.00_4.10_127_4000_5.04_turb.shad.jpg	1320	570	1410	850
43	2_8.00_4.10_98_5300_nan_turb.shad.jpg	1320	1100	1510	1350
44	2_9.00_4.10_90_37000_nan_shad.jpg	1330	1300	1480	1700
45	2_10.00_4.10_87_40000_5.17_refl.shad.jpg	1400	1450	1550	1900
46	2_11.00_4.10_84_71000_5.28_refl.shad.jpg	1400	750	1550	1200
47	2_12.00_4.10_86_52000_5.28_refl.shad.jpg	1400	750	1550	1000
48	2_15.00_4.10_72_28400_5.33_turb.shad.jpg	1300	1300	1400	1550
49	2_16.00_4.10_69_13700_5.32_turb.shad.jpg	1400	920	1550	1130
50	2_17.00_4.10_67_11900_5.36_turb.shad.jpg	1400	1200	1550	1400
51	2_6.00_03.10_160_150_5.33_refl.shad.jpg	1450	300	1600	1000
52	2_7.00_03.10_151_23200_nan_shad.jpg	1300	200	1450	800
53	2_8.00_03.10_144_106000_nan_refl.shad.jpg	1400	300	1550	800
54	2_9.00_03.10_129_14000_nan_shad.jpg	1450	0	1620	500
55	2_10.00_03.10_109_15600_nan_shad.jpg	1400	0	1580	800
56	2_11.00_3.10_97_13200_nan_refl.shad.jpg	1400	700	1560	1000
57	2_12.00_03.10_91_25700_5.35_shad.jpg	1350	0	1500	1000
58	2_15.00_3.10_63_22800_5.47_refl.shad.jpg	1350	0	1450	1000
59	2_16.00_3.10_61_23100_nan_refl.shad.jpg	1470	0	1620	700
60	2_17.00_3.10_59_4300_nan_refl.shad.jpg	1220	0	1350	1000

Table B.3: Crop coordinates for fieldwork images - part 2

Image Num.	left Red	upper Red	right Red	lower Red	left Green	upper Green	right Green	lower Green
1	1840	1460	1910	1490	1840	1390	1910	1420
2	1810	1610	1860	1650	1810	1530	1860	1560
3	1720	1690	1790	1720	1690	1620	1760	1650
4	1650	1610	1710	1650	1630	1550	1680	1580
5	1730	1640	1810	1690	1730	1570	1810	1620
6	1760	1670	1830	1710	1730	1600	1800	1640
7	1560	1580	1620	1610	1530	1510	1590	1540
8	1860	1720	1930	1760	1860	1640	1930	1680
9	1820	1610	1920	1640	1800	1540	1900	1570
10	1860	1510	1930	1550	1860	1430	1930	1470
11	2330	970	2380	1000	2250	940	2310	970
12	1710	1640	1760	1670	1660	1570	1710	1600
13	1610	1620	1660	1650	1580	1530	1630	1560
14	1850	2140	1900	2170	1810	2070	1860	2100
15	1850	1710	1910	1740	1810	1640	1880	1670
16	1730	1590	1810	1600	1720	1500	1800	1520
17	1730	1420	1800	1450	1800	1350	1850	1400
18	2140	1705	2180	1755	2090	1650	2130	1700
19	1900	1770	1950	1820	1850	1720	1900	1770
20	1450	1710	1510	1740	1420	1640	1480	1670
21	2040	1290	2080	1320	2000	1250	2040	1280
22	690	1570	730	1600	730	1600	770	1630
23	670	1590	710	1620	730	1590	770	1620
24	870	1740	910	1770	930	1740	970	1770
25	1080	1600	1110	1630	1130	1620	1160	1660
26	1080	1760	1110	1800	1120	1800	1150	1840
27	1160	1580	1190	1610	1200	1600	1240	1630
28	1490	1900	1520	1930	1550	1900	1580	1930
29	1270	1660	1300	1710	1320	1670	1350	1720
30	2370	570	2400	600	2410	600	2450	630
31	1070	1260	1130	1290	1070	1310	1130	1340
32	1420	1330	1450	1390	1370	1330	1400	1390
33	1100	1820	1130	1860	1170	1820	1200	1860
34	1280	1340	1340	1370	1280	1400	1340	1430
35	1350	1360	1380	1420	1400	1360	1430	1420
36	1440	1380	1490	1410	1440	1440	1490	1470
37	1310	1640	1340	1680	1350	1670	1390	1710
38	1370	1470	1400	1510	1420	1460	1450	1510
39	1350	1300	1380	1350	1410	1300	1440	1350
40	1080	1430	1110	1470	1110	1470	1140	1510
41	1430	1120	1480	1140	1430	1060	1480	1090
42	1340	1010	1400	1040	1340	950	1410	980
43	1340	890	1400	920	1320	840	1380	870
44	1390	1080	1420	1110	1360	1040	1390	1070
45	1350	1130	1380	1150	1320	1080	1350	1110
46	1470	1400	1500	1430	1470	1350	1500	1380
47	1390	1600	1420	1630	1370	1550	1400	1580
48	1260	1200	1290	1230	1230	1160	1260	1190
49	1470	1280	1500	1310	1440	1240	1480	1270
50	1470	1070	1500	1100	1440	1030	1470	1060
51	1690	1240	1720	1270	1640	1210	1680	1240
52	1420	1000	1470	1030	1400	950	1450	980
53	1540	1000	1590	1030	1500	950	1550	980
54	1470	730	1530	760	1470	670	1530	700
55	1400	1040	1460	1070	1400	1000	1460	1030
56	1470	1180	1500	1210	1450	1130	1490	1160
57	1370	1215	1430	1240	1370	1165	1430	1190
58	1370	1170	1440	1195	1370	1115	1440	1140
59	1570	915	1640	940	1570	860	1640	890
60	1270	1290	1350	1310	1270	1230	1350	1260

Table B.4: Crop coordinates for fieldwork images - part 3

Image Num.	**left Blue**	**upper Blue**	**right Blue**	**lower Blue**
1	1820	1310	1890	1340
2	1810	1460	1860	1490
3	1690	1550	1760	1580
4	1600	1480	1670	1510
5	1730	1500	1810	1540
6	1710	1530	1780	1570
7	1520	1440	1570	1470
8	1830	1580	1900	1620
9	1780	1470	1880	1500
10	1840	1360	1910	1400
11	2190	910	2240	940
12	1630	1500	1680	1530
13	1540	1480	1590	1510
14	1790	2000	1840	2030
15	1780	1580	1860	1600
16	1670	1450	1740	1470
17	1860	1320	1910	1350
18	2040	1600	2070	1650
19	1800	1660	1850	1700
20	1390	1570	1440	1600
21	1980	1210	2020	1240
22	790	1600	820	1630
23	780	1600	810	1630
24	980	1740	1020	1770
25	1180	1630	1210	1670
26	1160	1830	1190	1870
27	1250	1630	1280	1660
28	1600	1900	1630	1930
29	1370	1690	1400	1740
30	2440	630	2480	660
31	1070	1360	1130	1390
32	1320	1330	1350	1390
33	1210	1800	1240	1830
34	1280	1440	1340	1470
35	1450	1370	1480	1430
36	1440	1490	1490	1520
37	1400	1700	1430	1740
38	1470	1450	1500	1500
39	1450	1280	1480	1310
40	1150	1510	1180	1540
41	1430	1010	1480	1040
42	1340	900	1410	930
43	1300	800	1340	830
44	1340	1000	1370	1030
45	1260	1080	1290	1110
46	1430	1310	1460	1340
47	1370	1500	1400	1530
48	1200	1120	1230	1150
49	1410	1200	1440	1230
50	1400	1000	1430	1030
51	1590	1190	1630	1220
52	1380	900	1430	930
53	1470	910	1520	940
54	1470	620	1530	650
55	1400	940	1460	970
56	1440	1080	1470	1110
57	1370	1115	1430	1140
58	1370	1065	1430	1090
59	1570	805	1640	830
60	1270	1180	1350	1210

C

Code retrieving RGB intensities

```
import os
import pandas as pd
import numpy as np
import matplotlib.pyplot as plt
import matplotlib.image as mpimg
from PIL import Image
import cv2

from google.colab import drive
drive.mount('/content/drive')

## Directory to images

directory = '/content/drive/MyDrive/MDP/FW_10days/RGB_results/RGB_useful_photos'

# Get a list of image files in the directory
image_extensions = ('.jpg', '.jpeg', '.HEIC', '.heic')
image_files = [f for f in os.listdir(directory) if
f.lower().endswith(image_extensions)]

## Creating Dataframe

# Create a pandas DataFrame with the image titles
df = pd.DataFrame(image_files, columns=['Image_Title'])

# Use a regular expression to remove multiple extensions
df['Image_Title_cleaned'] = df['Image_Title'].str.replace(r'\.
(jpeg|jpg|HEIC|heic)$', '', regex=True, case=False)

# Split the cleaned Image_Title by '_'
df_split = df['Image_Title_cleaned'].str.split('_', expand=True)

# Assign the split columns to their respective names
col_names = ['Location␣[-]', 'Time␣[h]', 'Date␣[day.month]', 'Turbidtiy␣[NTU]',
'Light␣intensity␣[lux]', 'Distance␣camera-water␣[m]', 'Extra␣notes']
df_split.columns = col_names

# Convert 'Date [day.month]' to ensure proper two-digit day and month
df_split['Date␣[day.month]'] = df_split['Date␣[day.month]']
```

```
.apply(lambda x: '.'.join([f'{int(part):02}' for part in x.split('.')]))

# Convert 'Time [h]' to a proper format and replacing '.' with ':'
df_split['Time␣[h]'] = df_split['Time␣[h]'].str.replace('.', ':')

# Optionally, convert the data to numeric where necessary
df_split = df_split.apply(pd.to_numeric, errors='ignore')

# Add Image Titles in
df_split['Image_Title'] = df['Image_Title']

df_split.tail(50)

## Determining crop coordinates

from google.colab.patches import cv2_imshow

# Loading image
image_path = '/content/drive/MyDrive/MDP/FW_10days/RGB_results/RGB_useful_photos
/3_7.00_08.10_14.93_12315_3.75_refl.shad.jpg'
image = cv2.imread(image_path)

if image is None:
    print("Error:␣Could␣not␣load␣image.")
    exit()

height, width = image.shape[:2]
print(f"Image␣boundary␣values:␣Width␣=␣{width},␣Height␣=␣{height}")

# Define cropping box (left, upper, right, lower)
box = (1050, 200, 1200, 800)
left, upper, right, lower = box

# Check if box fits within image
if right > width or lower > height:
    print("Error:␣Cropping␣box␣exceeds␣image␣boundaries.")
else:
    cv2.rectangle(image, (left, upper), (right, lower), (0, 0, 255), 2)

    scale_factor = 0.3
    new_width = int(image.shape[1] * scale_factor)
    new_height = int(image.shape[0] * scale_factor)
    resized_image = cv2.resize(image, (new_width, new_height))

    cv2_imshow(resized_image)

## Giving access to goolge spreadsheet

from google.colab import auth
from googleapiclient.discovery import build
from google.auth.transport.requests import Request
import gspread
from google.auth import default

# Authenticate user
auth.authenticate_user()
```

```
# Connect to Google Sheets
creds, _ = default()
gc = gspread.authorize(creds)

## Loading in spreadsheet and adding DataFrame

# Loading Google Sheet
spreadsheet_url ='https://docs.google.com/spreadsheets/d
/11I_nMunAvRNbzhQ0jHxXkY1qCBZUIqJMiZK-RzZ8yTg/edit?gid=0#gid=0'

# Extract the sheet ID from the URL
sheet_id = spreadsheet_url.split('/')[5]

# Open the Google Sheet by sheet ID
sheet = gc.open_by_key(sheet_id)

# Select the worksheet by name (or index)
worksheet = sheet.worksheet('Blad1')  # Change 'Sheet1' to your sheet name

# Get all values from the sheet
data = worksheet.get_all_values()

crop = pd.DataFrame(data[1:], columns=data[0])
crop.head()

## Merging dataframes
# Assuming 'crop' is the first DataFrame and 'df_split' is the second DataFrame
merged_df = pd.merge(df_split, crop, on="Image_Title", how="left")

# Display the first few rows of the merged DataFrame
merged_df.head()

## Determining RGB intensities

# Paths
input_folder = '/content/drive/MyDrive/MDP/Experimenten/Sediment_experiment
/Photos_sed_exp'
output_folder = '/content/drive/MyDrive/MDP/Experimenten/Sediment_experiment
/Photos_sed_exp_cropped_0'

# Ensure the output folder exists
if not os.path.exists(output_folder):
    os.makedirs(output_folder)

# Function to calculate the sum of R, G, B values and pixel count
def calculate_rgb_sums(image):
    # Convert the image to a NumPy array
    img_array = np.array(image)

    # Get pixel count
    pixel_count = img_array.shape[0] * img_array.shape[1]

    # If the image is RGB, calculate the sum for each channel (R, G, B)
    if img_array.ndim == 3:  # RGB image
        sum_R = img_array[:, :, 0].sum()
```

```
        sum_G = img_array[:, :, 1].sum()
        sum_B = img_array[:, :, 2].sum()
    else:
        sum_R = sum_G = sum_B = img_array.sum()
    return sum_R, sum_G, sum_B, pixel_count

# Function to crop and save an image, also return the cropped image
def crop_and_save(image_title, output_name, left, upper, right, lower):
    input_path = os.path.join(input_folder, image_title)
    output_path = os.path.join(output_folder, output_name)

    try:
        # Open the image
        img = Image.open(input_path)

        # Define the region to crop (left, upper, right, lower)
        box = (left, upper, right, lower)

        # Crop the image
        img_cropped = img.crop(box)

        # Save the cropped image
        img_cropped.save(output_path)

        print(f"Cropped image saved: {output_path}")

        return img_cropped  # Return the cropped image for further processing

    except Exception as e:
        print(f"Error cropping {image_title}: {e}")
        return None

# Convert the cropping columns to numeric (floats or ints), handling errors
numeric_columns = ['left', 'upper', 'right', 'lower']

# Convert the columns, setting invalid values to NaN
crop[numeric_columns] = crop[numeric_columns].apply(pd.to_numeric, errors='coerce')

# Iterate over DataFrame rows, crop images, and calculate RGB sums and averages
for index, row in crop.iterrows():
    image_title = row['Image_Title']  # Image title in the DataFrame

    # Create unique output names for each crop
    output_name_RGB = f"cropped_RGB_{image_title}"
    output_name_R = f"cropped_R_{image_title}"
    output_name_G = f"cropped_G_{image_title}"
    output_name_B = f"cropped_B_{image_title}"

    # Initialize columns in the DataFrame for sums, pixel counts, and averages
    crop.at[index, 'sum_R_RGB'] = crop.at[index, 'sum_G_RGB']
    = crop.at[index, 'sum_B_RGB'] = np.nan
    crop.at[index, 'sum_R_R'] = crop.at[index, 'sum_G_R']
    = crop.at[index, 'sum_B_R'] = np.nan
    crop.at[index, 'sum_R_B'] = crop.at[index, 'sum_G_B']
    = crop.at[index, 'sum_B_B'] = np.nan
    crop.at[index, 'sum_R_G'] = crop.at[index, 'sum_G_G']
```

```
= crop.at[index, 'sum_B_G'] = np.nan
crop.at[index, 'Cropped␣pixel_count_RGB']
= crop.at[index, 'Cropped␣pixel_count_R'] = crop.at[index, 'Cropped␣pixel_count_G']
= crop.at[index, 'Cropped␣pixel_count_B'] = np.nan

crop.at[index, 'avg_R_RGB'] = crop.at[index, 'avg_G_RGB']
= crop.at[index, 'avg_B_RGB'] = crop.at[index, 'avg_RGB_RGB'] = np.nan
crop.at[index, 'avg_R_R'] = crop.at[index, 'avg_G_R']
= crop.at[index, 'avg_B_R'] = crop.at[index, 'avg_RGB_R'] = np.nan
crop.at[index, 'avg_R_G'] = crop.at[index, 'avg_G_G']
= crop.at[index, 'avg_B_G'] = crop.at[index, 'avg_RGB_G'] = np.nan
crop.at[index, 'avg_R_B'] = crop.at[index, 'avg_G_B']
= crop.at[index, 'avg_B_B'] = crop.at[index, 'avg_RGB_B'] = np.nan

# Crop and save using the provided RGB values
img_cropped_RGB = crop_and_save(image_title, output_name_RGB, row['left_RGB'],
row['upper_RGB'], row['right_RGB'], row['lower_RGB'])
img_cropped_R = crop_and_save(image_title, output_name_R, row['left_R'],
row['upper_R'], row['right_R'], row['lower_R'])
img_cropped_G = crop_and_save(image_title, output_name_G, row['left_G'],
row['upper_G'], row['right_G'], row['lower_G'])
img_cropped_B = crop_and_save(image_title, output_name_B, row['left_B'],
row['upper_B'], row['right_B'], row['lower_B'])

# If images successfully cropped, calculate RGB sums, pixel count, and averages
if img_cropped_RGB is not None:
    sum_R, sum_G, sum_B, pixel_count = calculate_rgb_sums(img_cropped_RGB)
    crop.at[index, 'sum_R_RGB'] = sum_R
    crop.at[index, 'sum_G_RGB'] = sum_G
    crop.at[index, 'sum_B_RGB'] = sum_B
    crop.at[index, 'Cropped␣pixel_count_RGB'] = pixel_count
    # Calculate averages
    crop.at[index, 'avg_R_RGB'] = sum_R / pixel_count if pixel_count > 0
    else np.nan
    crop.at[index, 'avg_G_RGB'] = sum_G / pixel_count if pixel_count > 0
    else np.nan
    crop.at[index, 'avg_B_RGB'] = sum_B / pixel_count if pixel_count > 0
    else np.nan

    # Calculate average RGB
    crop.at[index, 'avg_RGB_RGB'] = ((sum_R / pixel_count) +
    (sum_G / pixel_count) + (sum_B / pixel_count))/3
    if pixel_count > 0 else np.nan

if img_cropped_R is not None:
    sum_R, sum_G, sum_B, pixel_count = calculate_rgb_sums(img_cropped_R)
# Only R channel
    crop.at[index, 'sum_R_R'] = sum_R
    crop.at[index, 'sum_G_R'] = sum_G
    crop.at[index, 'sum_B_R'] = sum_B
    crop.at[index, 'Cropped␣pixel_count_R'] = pixel_count
    # Calculate average R
    crop.at[index, 'avg_R_R'] = sum_R / pixel_count if pixel_count > 0
    else np.nan
    crop.at[index, 'avg_G_R'] = sum_G / pixel_count if pixel_count > 0
    else np.nan
```

```
        crop.at[index, 'avg_B_R'] = sum_B / pixel_count if pixel_count > 0
        else np.nan

        # Calculate average RGB
        crop.at[index, 'avg_RGB_R'] = ((sum_R / pixel_count) +
        (sum_G / pixel_count) + (sum_B / pixel_count))/3
        if pixel_count > 0 else np.nan

    if img_cropped_G is not None:
        sum_R, sum_G, sum_B, pixel_count = calculate_rgb_sums(img_cropped_G)
# Only G channel
        crop.at[index, 'sum_R_G'] = sum_R
        crop.at[index, 'sum_G_G'] = sum_G
        crop.at[index, 'sum_B_G'] = sum_B
        crop.at[index, 'Cropped␣pixel_count_G'] = pixel_count
        # Calculate average G
        crop.at[index, 'avg_R_G'] = sum_R / pixel_count
        if pixel_count > 0 else np.nan
        crop.at[index, 'avg_G_G'

## Define the output Excel file path

output_excel_file = '/content/drive/MyDrive/MDP/FW_10days/RGB_results
/merged_output.xlsx'

# Save the DataFrame to an Excel file
merged_df.to_excel(output_excel_file, index=False)

print(f"DataFrame␣saved␣to␣{output_excel_file}")
```

D

Results RGB images constructions

D.1 Location 2 - RGB images results

Figure D.1: Time fluctuations of Location 2 - 03/10/24 and 04/10/24

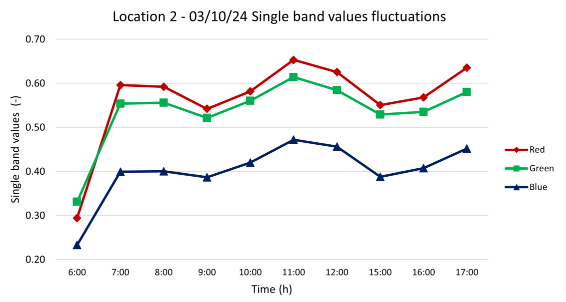

Figure D.2

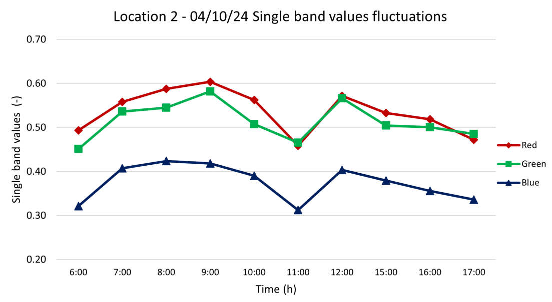

Figure D.3

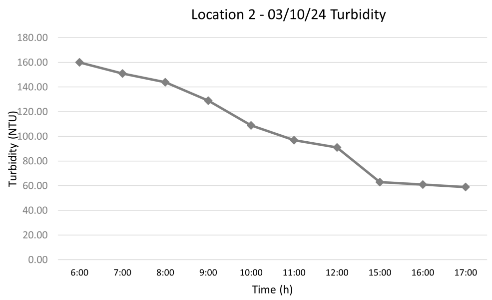

Figure D.4

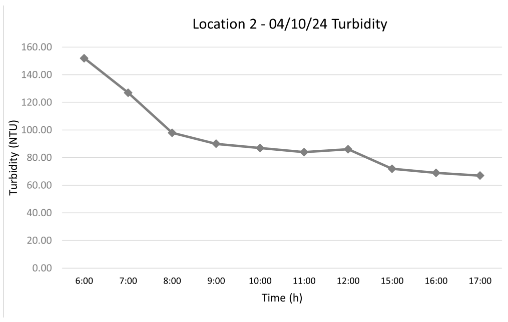

Figure D.5

Figure D.6: Correlations of PI and TSS for Location 2 - 03/10/24 and 04/10/24

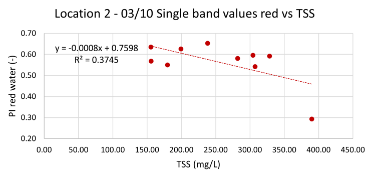

Figure D.7

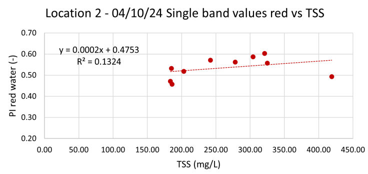

Figure D.8

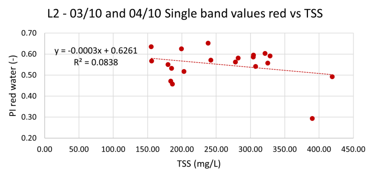

Figure D.9

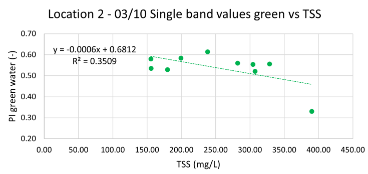

Figure D.10

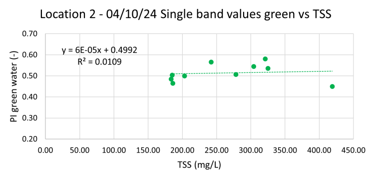

Figure D.11

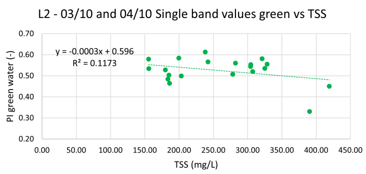

Figure D.12

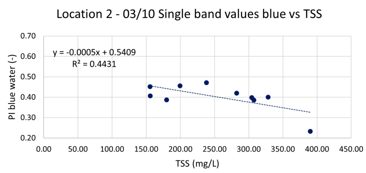

Figure D.13

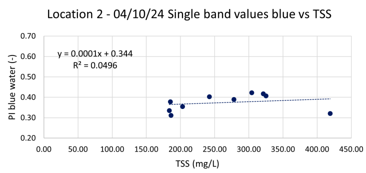

Figure D.14

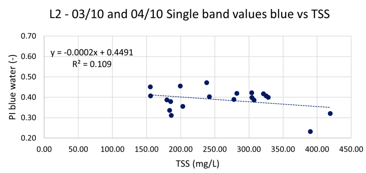

Figure D.15

D.2 Location 3 - RGB images results

Figure D.16: Time fluctuations of Location 3 - 07/10/24 and 08/10/24

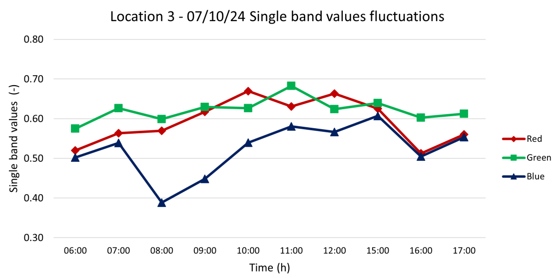

Figure D.17

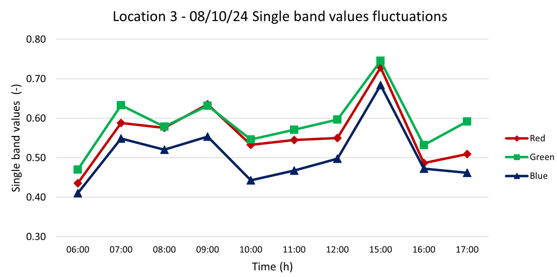

Figure D.18

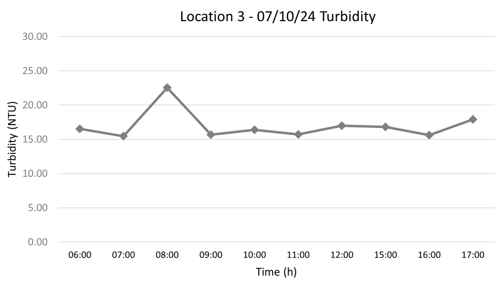

Figure D.19

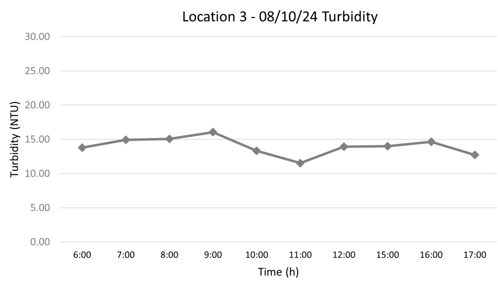

Figure D.20

Figure D.21: Correlations of PI and TSS for Location 3 - 07/10/24 and 08/10/24

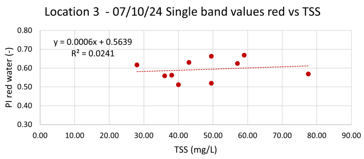

Figure D.22

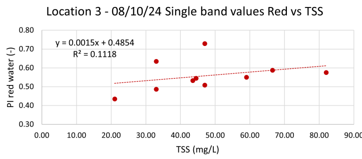

Figure D.23

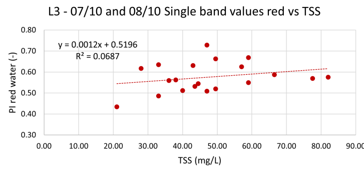

Figure D.24

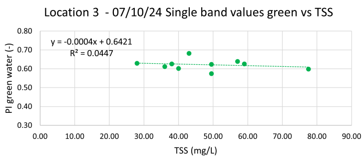

Figure D.25

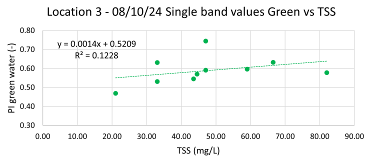

Figure D.26

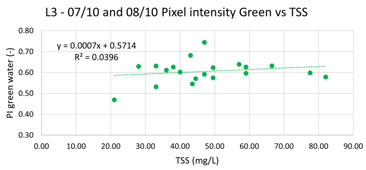

Figure D.27

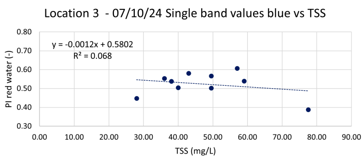

Figure D.28

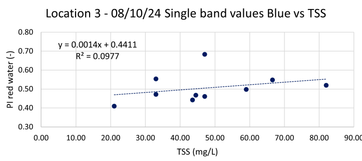

Figure D.29

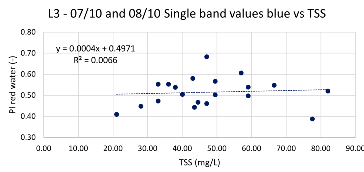

Figure D.30

E

TSS deposit

particle size	particle density	settling velocity V	settlings distance Ds(m)	settling efficienty	settled TSS mg/s	settled TSS kg per year	m^3 per year
0.00236	2400	0.6	2075.5	100.0000	263200000.0	830027520.0	345844.8
0.001	2400	0.1	372.7	100.0000	263200000.0	830027520.0	345844.8
0.000425	2200	0.0	57.7	100.0000	263200000.0	830027520.0	377285.2
0.00018	2200	0.0	10.4	100.0000	263200000.0	830027520.0	377285.2
0.00015	2200	0.0	7.2	100.0000	263200000.0	830027520.0	377285.2
0.000106	2200	0.0	3.6	100.0000	263200000.0	830027520.0	377285.2
0.000075	2200	0.0	1.8	71.9201	189293760.0	596956801.5	271344.0
0.000063	1700	0.0	0.7	29.7075	78190189.1	246580580.2	145047.4
avg discharge Loc 1	14	m^3/s					
Volume Loc 1	48000	m^3					
rho_f	994	kg/m^3					
g	9.81	m/s^2					
mu	0.00705	Pa-s					
h	2.5	m					
Hydraulic resedince time (HRT) Loc 1	3428.571429	s					
TSS concentration Loc 1 avg	188	mg/L					
TSS concentration Loc 1 avg	188000	mg/m3					

Figure E.1

particle size	particle density	settling velocity V	settlings distance Ds (m)	settling efficienty	settled TSS mg/s	settled TSS kg per year	m^3 per year	
0.00236	2400	0.6	9121925.8	100.0000	1387000.0	4374043.2	1822.5	
0.001	2400	0.1	1637806.3	100.0000	1387000.0	4374043.2	1822.5	
0.000425	2200	0.0	253747.9	100.0000	1387000.0	4374043.2	1988.2	
0.00018	2200	0.0	45516.6	100.0000	1387000.0	4374043.2	1988.2	
0.00015	2200	0.0	31608.7	100.0000	1387000.0	4374043.2	1988.2	
0.000106	2200	0.0	15784.7	100.0000	1387000.0	4374043.2	1988.2	
0.000075	2200	0.0	7902.2	100.0000	1387000.0	4374043.2	1988.2	
0.000063	1700	0.0	3264.1	100.0000	1387000.0	4374043.2	2573.0	
							16159.0	total
avg discharge reservoir A	0.73	m^3/s						
Volume reservoir A	11000000	m^3						
rho_f	994	kg/m^3						
g	9.81	m/s^2						
mu	0.00705	Pa-s						
h	10	m						
Hydraulic resedince time (HRT)	15068493.15	s						
TSS concentration	19	mg/L						
TSS concentration	19000	mg/m3						

Figure E.2

particle size	particle density	settling velocity Vs	settlings distance Ds (m)	settling efficienty	settled TSS mg/s	settled TSS kg per year	m^3 per year
0.00236	2400	0.6053642	536.9	100.0000	255680000.0	806312448.0	335963.5
0.001	2400	0.1086908	96.4	100.0000	255680000.0	806312448.0	335963.5
0.000425	2200	0.0168396	14.9	100.0000	255680000.0	806312448.0	366505.7
0.00018	2200	0.0030206	2.7	100.0000	255680000.0	806312448.0	366505.7
0.00015	2200	0.0020977	1.9	100.0000	255680000.0	806312448.0	366505.7
0.000106	2200	0.0010475	0.9	54.6510	139731614.0	440657618.1	200298.9
0.000075	2200	0.0005244	0.5	27.3595	69952859.5	220603337.6	100274.2
0.000063	1700	0.0002166	0.2	11.3012	28894916.1	91123007.3	53601.8
avg discharge reservoir A	13.6	m^3/s					
Volume reservoir A	12062	m^3					
rho_f	994	kg/m^3					
g	9.81	m/s ^2					
mu	0.00705	Pa-s					
h	1.7	m					
Hydraulic resedince time (HRT)	886.9117647	s					
TSS concentration	188	mg/L					
TSS concentration	188000	mg/m3					

Figure E.3

F
Characteristics Deeper Pro+ 2

Technical Specifications

Weight: 3.5oz / 100g
Size: 65mm / 2.5in in Diameter
Sonar Type: Dual Beam
Frequency (Beam cone): 290 kHz, 15° and 90 kHz, 55°
Depth Range Max/Min: Max 260ft / 80 m, Min 2ft / 0.5m
Sonar Scan rate: Up to 15 scans per second
Operating Temperature: -20°C to 40°C / -4°F to 104°F
Internal Battery: Lithium Polymer, 3.7V Rechargeable, 850mAh
Power Supply input: Micro USB B type, 5V DC, 450mA max
(for charging battery)
Power Adapter Input: AC 110V/240V. Output Micro USB, 5V 450mAh
Wireless connection type: Wi-Fi
GPS Positioning: L1 48 channel GPS receiver, high 3m@50% accuracy
Casting Range: Up to 330ft / 100m. Range depends on the OS and smartphone model
Battery Life: Up to 6 hours
Charging Time: 2 hours
Device compatibility: Android 7.0 or later, iOS 13.0 or later.

Figure F.1: Specifications Deeper 2 Pro [19]

G

Locations Cross sections reservoirs

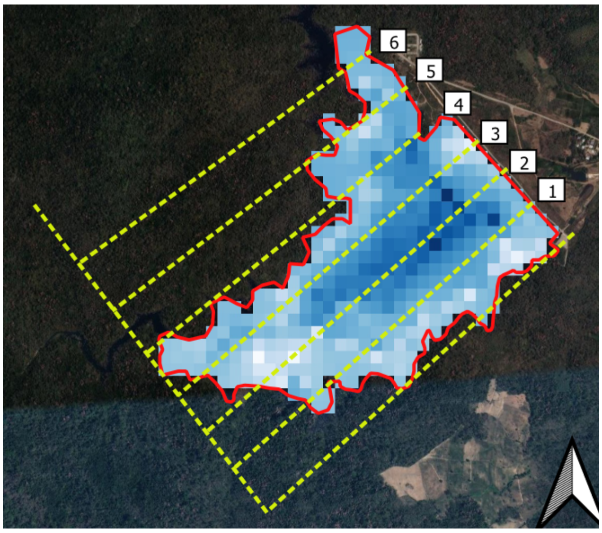

Figure G.1: Location Cross Section Reservoir A

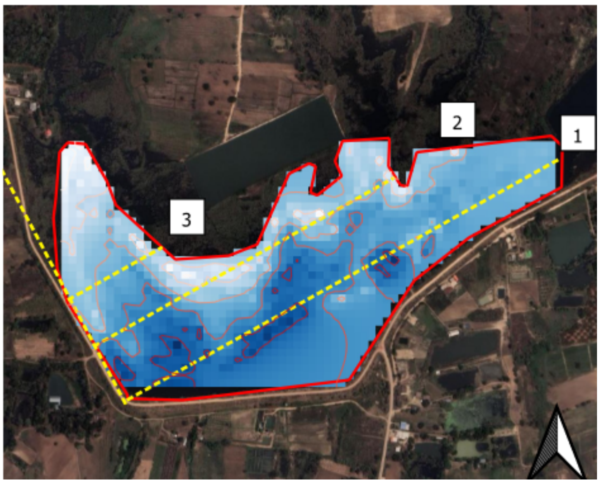

Figure G.2: Location Cross Section Reservoir B

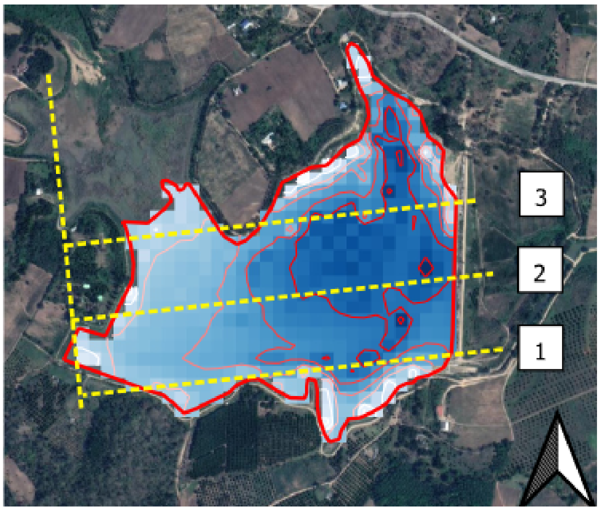

Figure G.3: Location Cross Section Reservoir C

H

Reference point Location B

coordinates: 16.490471, 99.309137
Distance between reference point and water level: 6.35m

Figure H.1: Measured distance reference point to water level

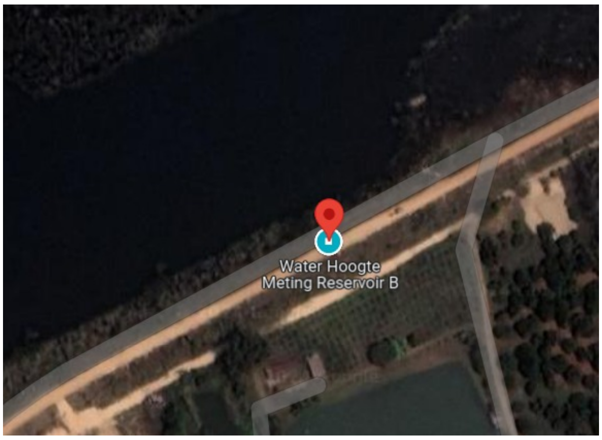

Figure H.2: Location reference point

Bibliography

[1] Deeper Pro 2+. Deeper pro 2+ castable and portable wireless fishfinder, 2024. URL https://www.amazon.com/Deeper-Castable-Portable-Wireless-Fishfinder/dp/B09BD7YYBJ. Accessed: 2024-10-23.

[2] Deeper Pro+ 2 App. Deeper pro+ 2 wireless fishfinder app, 2024. URL https://buydeeper.ru/besprovodnoy-eholot-deeper-sonar-pro-plus-2. Accessed: 2024-10-23.

[3] Lei Cheng, Xiyue Tan, Dong Yao, Wenxia Xu, Huaiyu Wu, and Yang Chen. A fishery water quality monitoring and prediction evaluation system for floating uav based on time series. *Sensors*, 21 (13):4451, 2021. URL https://doi.org/10.3390/s21134451. Accessed: 2024-11-06.

[4] L. Daniels, E. Eeckhout, J. Wieme, Y. Dejaegher, K. Audenaert, and W. H. Maes. Identifying the optimal radiometric calibration method for uav-based multispectral imaging. *Remote Sensing*, 15(11):2909, 2023. doi: 10.3390/rs15112909. URL https://doi.org/10.3390/rs15112909.

[5] Lateiro Salvador de Sousa, Raphael Muli Wambua, James Messo Raude, and Benedict Mwavu Mutua. Assessment of water flow and sedimentation processes in irrigation schemes for decision-support tool development: A case review for the chókwè irrigation scheme, mozambique. *AgriEngineering*, 1(1):100–118, 2019. ISSN 2624-7402. doi: 10.3390/agriengineering1010008. URL https://www.mdpi.com/2624-7402/1/1/8.

[6] Erik Delaquis, Stef de Haan, and Kris A.G. Wyckhuys. On-farm diversity offsets environmental pressures in tropical agro-ecosystems: A synthetic review for cassava-based systems. *Agriculture, Ecosystems and Environment*, 251:226–235, 2018. ISSN 0167-8809. doi: https://doi.org/10.1016/j.agee.2017.09.037. URL https://www.sciencedirect.com/science/article/pii/S0167880917304449.

[7] Jin Fan and Gregory L. Morris. Reservoir sedimentation. ii: Reservoir deposition patterns. *Journal of Hydraulic Engineering*, 118(3):370–384, 1992.

[8] Khaled Hassaballah, Ahmed Nagy, and Sayed R. Abdrabbo. The impact of blockage on the performance of canal coverage structures. *Journal of Engineering and Applied Science*, 70 (1):45, 2023. doi: 10.1186/s44147-023-00246-0. URL https://doi.org/10.1186/s44147-023-00246-0.

[9] Think Hazard. Khlong lan - landslide risk report, 2023. URL https://thinkhazard.org/en/report/26565-thailand-kampaeng-phet-khlong-lan/LS. Accessed: October 20, 2024.

[10] K. Jia, U. Hasan, H. Jiang, B. Qin, S. Chen, D. Li, and J. Shen. How frequent the landsat 8/9-sentinel 2a/b virtual constellation observed the earth for continuous time series monitoring. *International Journal of Applied Earth Observation and Geoinformation*, 130:103899, 2024. doi: 10.1016/j.jag.2023.103899.

[11] T. Leeuw and E. Boss. The hydrocolor app: Above water measurements of remote sensing reflectance and turbidity using a smartphone camera. *Sensors*, 18(1):256, 2018. doi: 10.3390/s18010256. URL https://www.mdpi.com/1424-8220/18/1/256. Accessed: 2024-10-23.

[12] Y. Liu and H. Zhang. Sediment concentration retrieval from rgb images using a controlled lighting setup. *Remote Sensing*, 11(17):1955, 2019. doi: 10.3390/rs11171955.

[13] Salvatore Manfreda, Domenico Miglino, Khim Cathleen Saddi, Seifeddine Jomaa, Anette Eltner, Matthew Perks, Salvador Peña-Haro, Thom Bogaard, Tim H.M. van Emmerik, Stefano Mariani, Ian Maddock, et al. Advancing river monitoring using image-based techniques: challenges and opportunities. *Hydrological Sciences Journal*, 69, 2024. doi: 10.1080/02626667.2024.2333846. URL https://doi.org/10.1080/02626667.2024.2333846.

[14] D. Miglino, K. C. Saddi, F. Isgrò, S. Jomaa, M. Rode, and S. Manfreda. Image processing for continuous river turbidity monitoring: Full-scale tests and potential applications. *Science of the Total Environment*, 2024.

[15] A. Nayak et al. Title of the paper. *Remote Sensing*, 15(23):5540, 2023. doi: 10.3390/rs15235540.

[16] Duminda Perera, Spencer Williams, and Vladimir Smakhtin. Present and future losses of storage in large reservoirs due to sedimentation: A country-wise global assessment. *Sustainability*, 15 (1), 2023. ISSN 2071-1050. doi: 10.3390/su15010219. URL https://www.mdpi.com/2071-1050/15/1/219.

[17] A. Popradit et al. Soil degradation and herbicide pollution by repeated cassava monoculture within thailand's conservation region. *PLOS ONE*, 18(10):e0308284, 2023. doi: 10.1371/journal.pone.0308284. URL https://journals.plos.org/plosone/article?id=10.1371/journal.pone.0308284.

[18] Vasyl Sagan et al. A review on water quality monitoring and remote sensing techniques. *Frontiers in Environmental Science*, 10:1–20, 2020. doi: 10.3389/fenvs.2022.979133. URL https://www.frontiersin.org/journals/environmental-science/articles/10.3389/fenvs.2022.979133/full. Accessed: October 20, 2024.

[19] Deeper Support. What are the technical specs of the deeper smart sonar pro+? URL https://support.deeper.eu/073772-What-are-the-technical-specs-of-the-Deeper-Smart-Sonar-PRO. Retrieved November 2024.